2017

Site characterisation for the Ballina field testing facility

Richard B. Kelly
SMEC Australia, University of Newcastle, University of Wollongong

Jubert Pineda
University of Newcastle

L. Bates
University of Newcastle

L Suwal
University of Newcastle

A Fitzallen
Coffey Geotechnics

Site characterisation for the Ballina field testing facility

Abstract

A soft soil field testing facility has been recently established near Ballina, New SouthWales, on the east coast of Australia, which is aimed at improving design and construction methods for transport infrastructure. Several sampling, laboratory and in situ testing campaigns have been performed to characterise the material properties of the soil. High-quality laboratory testing has been performed at one location through the soil profile and a range of geophysics, cone penetrometer, seismic dilatometer, shear vane and permeability tests have been carried out at other locations. The in situ tests have demonstrated that the stratigraphy and test data are reasonably uniform across the site. Seasonal groundwater variations cause the in situ stress state to vary with time. In situ test data have been compared with laboratory tests in order to estimate soil material properties at the locations of the in situ tests. The accuracy of published correlations was variable and site-specific correlations were found to provide a better outcome. The coefficient of consolidation and the water permeability obtained from small-scale laboratory tests shows good agreement with in situ estimations based on piezocone penetration test (CPTu) dissipation tests and BAT tests, respectively. The correlation between laboratory and in situ data is used to develop a robust geotechnical model for the Ballina site.

Disciplines

Engineering | Science and Technology Studies

Publication Details

Kelly, R. B., Pineda, J. A., Bates, L., Suwal, L. P. & Fitzallen, A. (2017). Site characterisation for the Ballina field testing facility. Geotechnique: international journal of soil mechanics, 67 (4), 279-300.

Kelly, R. B. *et al*. (2017). *Géotechnique* **67**, No. 4, 279–300 [http://dx.doi.org/10.1680/jgeot.15.P.211]

Site characterisation for the Ballina field testing facility

R. B. KELLY*†‡, J. A. PINEDA†, L. BATES†, L. P. SUWAL† and A. FITZALLEN§

A soft soil field testing facility has been recently established near Ballina, New South Wales, on the east coast of Australia, which is aimed at improving design and construction methods for transport infrastructure. Several sampling, laboratory and in situ testing campaigns have been performed to characterise the material properties of the soil. High-quality laboratory testing has been performed at one location through the soil profile and a range of geophysics, cone penetrometer, seismic dilatometer, shear vane and permeability tests have been carried out at other locations. The in situ tests have demonstrated that the stratigraphy and test data are reasonably uniform across the site. Seasonal groundwater variations cause the in situ stress state to vary with time. In situ test data have been compared with laboratory tests in order to estimate soil material properties at the locations of the in situ tests. The accuracy of published correlations was variable and site-specific correlations were found to provide a better outcome. The coefficient of consolidation and the water permeability obtained from small-scale laboratory tests shows good agreement with in situ estimations based on piezocone penetration test (CPTu) dissipation tests and BAT tests, respectively. The correlation between laboratory and in situ data is used to develop a robust geotechnical model for the Ballina site.

KEYWORDS: clays; in situ testing; laboratory tests; penetrometers; site investigation; soil classification

INTRODUCTION

The concept of a soft soil field testing facility was promoted by the Ballina Bypass Alliance due to the difficulties encountered during the construction of a nearby motorway near Ballina, New South Wales on the east coast of Australia. Up to 6·4 m of embankment settlement had occurred over a period of 3 years during construction (maximum 14 m high fill) and accurate predictions of settlement, time rate of settlement and lateral soil movements had proved to be difficult. The Australian Research Council Centre of Excellence for Geotechnical Science and Engineering (CGSE) developed the concept and established the soft soil field testing facility. The motivation for establishing the field testing facility was to improve construction of transport infrastructure on natural soft soil deposits, which are commonly found along the eastern and southern Australian coastlines. There is currently 150 km of motorway in the process of construction in the general vicinity of Ballina, 25 km of which traverses soft soils. The performance of embankments constructed on soft clay is a key aspect of these works. However, predicting embankment deformations is challenging and frequently can be inaccurate, leading to increased costs during construction (e.g. Kelly, 2014). Extensive site investigations were performed by the Ballina Bypass Alliance along the alignment of the motorway and the test site was known to be underlain by deposits of soft estuarine clay to depths greater than 10 m. The combination of access to the site, ground conditions and proximity to construction equipment in Ballina made the location ideal for a test facility.

Manuscript received 21 September 2015; revised manuscript accepted 6 September 2016. Published online ahead of print 10 November 2016.
Discussion on this paper closes on 1 September 2017, for further details see p. ii.
* SMEC Australia, Brisbane, Australia.
† ARC Centre of Excellence for Geotechnical Science and Engineering, The University of Newcastle, Callaghan, Newcastle, Australia.
‡ University of Wollongong, Wollongong, Australia.
§ Coffey Geotechnics, Chatswood, Australia.

The site is located to the north west of the town of Ballina and occupies 6·5 ha of land that was previously used to farm sugar cane. Fig. 1(a) shows the location of the site within the regional geological setting. Fig. 1(b) shows a plan view of the site. At the time of acquisition, a hardstand and stockpile of fill materials had been placed at the southern end of the site by the Ballina Bypass Alliance, whereas the remainder of the site was greenfield. The ground surface is essentially flat with a level about 0·5 m Australian height datum (AHD). A value of 0·000 m AHD corresponds to mean sea level for 1966–1968 at 30 tide gauges around the coast of the Australian continent. The ground level reduces slightly to about 0·3 m AHD at the northern and eastern sides of the site adjacent to Emigrant and Fishery creeks, respectively. An open channel cane drain runs along the western boundary of the site and a series of shallow open drains run east–west across the site at about 15 m intervals. The tidal range is about ±1 mAHD at Ballina but may vary at the location of the test site. Small bunds, about 1 m high, were constructed by the farmers next to the creeks to prevent tidal flooding from having an impact on sugar farming. The bunds do not prevent large-scale flooding. The ground is not traversible when wet and a 1·5 m thick access track was constructed along the western boundary prior to performing the site characterisation.

An initial site characterisation study was performed prior to constructing two trial embankments, the results of which are discussed in this paper. The aims of the study were to assess the site stratigraphy, and to obtain high-quality soil samples for laboratory testing and for the development of geological and geotechnical models. Results from the advanced laboratory tests are discussed in a companion paper by Pineda *et al*. (2016a). A wide variety of in situ test results including piezocone penetration test (CPTu), seismic dilatometer testing (SDMT), field vane, BAT permeability tests and geophysical profiles are discussed in this paper. Additional in situ tests have been performed by partner investigators at the site including those from a hydrostatic profile tool, T-bar and piezoball (Colreavy *et al*., 2016), self-boring pressuremeter (Gaone *et al*., 2016) and penetrometers installed over a wide range of insertion rates. The results from

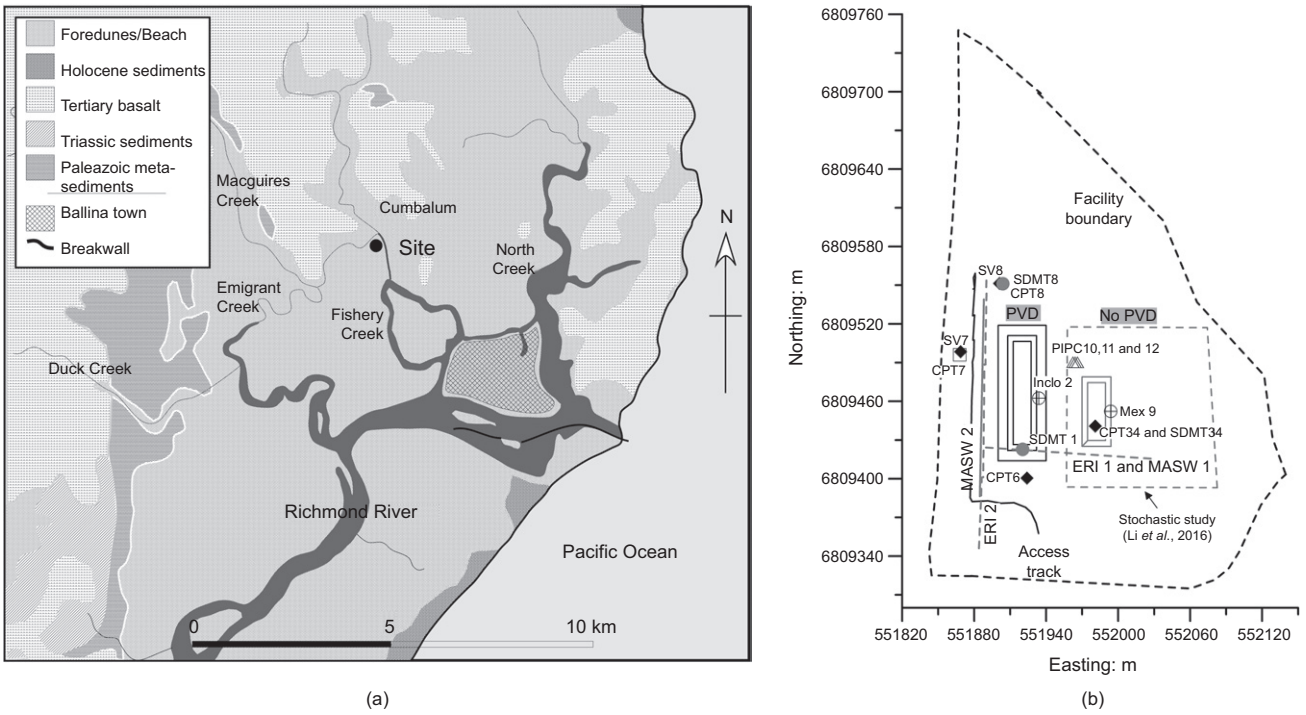

Fig. 1. (a) Geological setting (after Bishop, 2004). (b) Site plan

these supplementary in situ testing campaigns are not reported in this paper.

GEOLOGICAL SETTING AND GEOMORPHOLOGY

The location of the site in the regional geological setting is shown in Fig. 1(a). The adjacent hillsides are composed of basalt rock overlying Palaeozoic meta-sediments (argillite). A tuffaceous clay layer occasionally occurs between the basalt and the argillite. The basalt has been weathered to residual soil in its upper horizon. The basalt initially weathers to an aluminium, magnesium and iron montmorillonite, then to poorly crystalline montmorillonite and then to kaolinite/halloysite. If potassium is present, the montmorillonite can form illite and interstratified illite/smectite. Illite is also found in the argillaceous rocks (Loughnan, 1969). The formation of clay minerals is favoured by the relatively high temperature in the area. Extensive and rapid leaching of minerals occurs due to the high rainfall in the Ballina region and due to the permeable nature of the basalt rock (Loughnan, 1969). Therefore, it would be expected that the sediments at the soft soil field testing facility would have a high proportion of clay particles and the dominant clay minerals would be smectite, illite and kaolinite. Particle size distribution tests and X-ray diffraction tests carried out by Pineda *et al*. (2016a) support this interpretation. They reported kaolinite, illite and interstratified illite/smectite (also known as illite-bearing smectite) as the main clayey constituents of specimens from borehole Inclo 2.

The sea level at the time of the last glacial maximum, approximately 18 000 years BP, has been estimated at −130 m below current sea level. The sea level rose to 1·5 m to 2·0 m above current levels at about 8000 years BP, was constant at this level until 2000 to 3000 years BP and then reduced to current levels at the present time (Lewis *et al*., 2013). Quaternary deposition sequences were identified by Bishop (2004) for deposits in the Richmond River valley. Initial deposition occurred during the Pleistocene Age and comprised 1 m to 2 m thick deposits of fluvial sandy gravels overlain by very stiff oxidised clays. These deposits have been eroded and exist generally from bedrock to reduced level (RL)−15 m AHD. A highly oxidised and indurated alteration horizon overlies the Pleistocene deposits at some locations. Palaeochannels were eroded through the stiff clay deposits, one of which exists below Fishery creek immediately to the east of the soft soil field testing facility. As the sea levels rose, the Richmond River estuary was filled with Holocene Age sediments that formed behind a barrier dune complex. These sediments grade from gravels and sandy clays at lower levels to dark grey shelly muds in the upper levels. Deposits above RL−10 m AHD comprise mainly clays. Bishop (2004) infers that the presence of interbedded estuarine sands and muds below RL−10 m AHD indicates deposition under high-energy conditions. The absence of sands above RL−10 m AHD was interpreted to correspond with the formation of a coastal barrier that created a low-energy estuarine depositional environment behind it. The RL−10 m AHD level occurred between 8000 and 9000 years BP.

The estuary is inferred to be filled in a highly heterogeneous process due to differences in sedimentation rates across the fluvial delta. A delta plain was rapidly established near the mouth of the Richmond River. Cut-off and interchannel bays are thought to have evolved from the unfilled remnants of the original estuarine basin away from the delta, which persisted after formation of the delta (Hashimoto *et al*., 2006). The location of the field testing facility appears to be sufficiently distant from the coastal barrier that the sediments would have been mostly deposited under water. This interpretation is supported by the lack of sand lenses within the estuarine clay. However, based on oedometer test results obtained near the Richmond River south of Ballina, Bishop & Fityus (2006) inferred that the clays above about 4 m depth were deposited in a tidal flat environment while clays below 4 m depth were considered to be deposited in the less dynamic deeper water environment. A last stage of deposition associated with flooding has occurred since the sea level has fallen. These sediments are composed of sands, silts and clays. Electrical conductivity measurements performed on the pore water (Fig. 2(d)) indicate that the pore

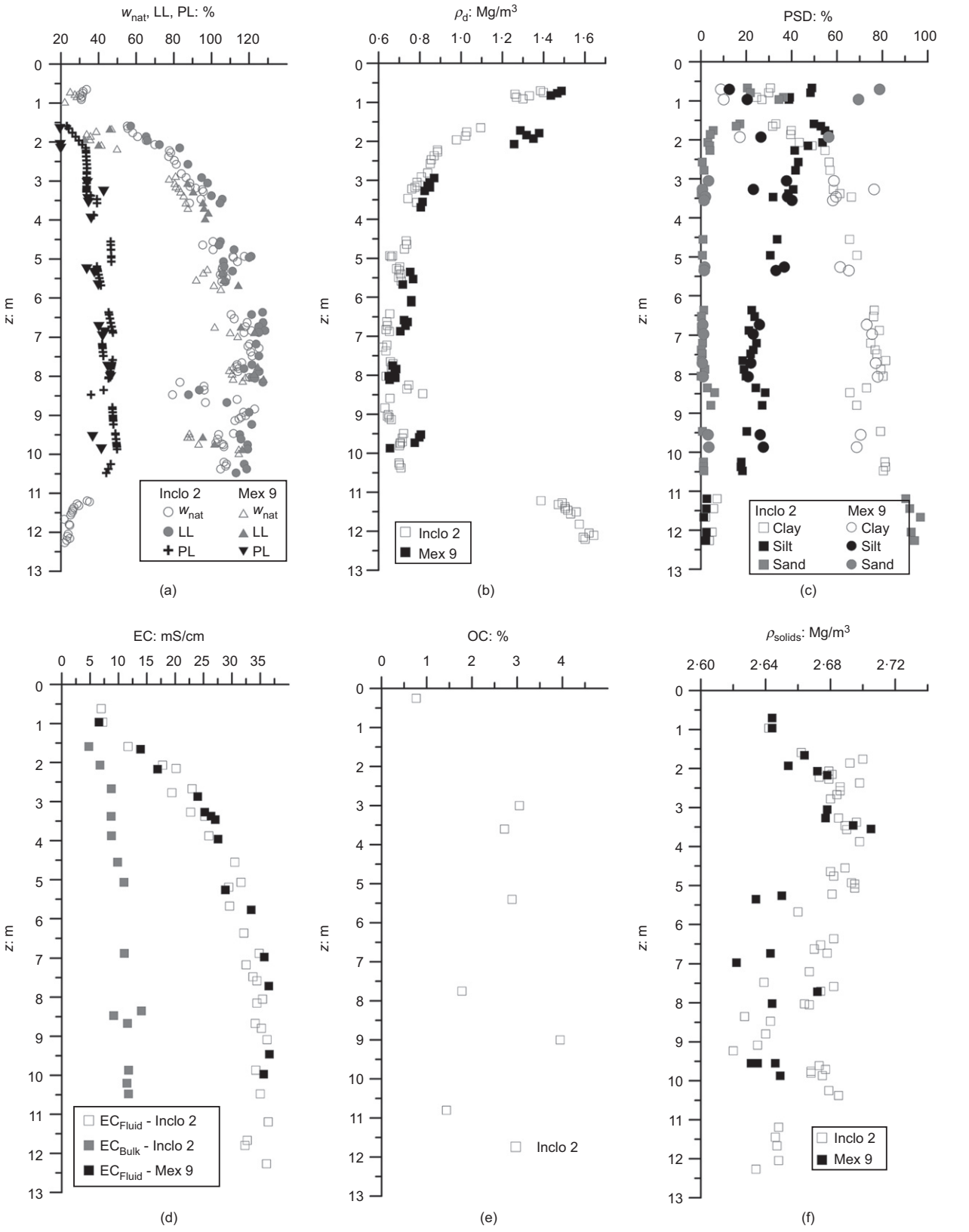

Fig. 2. Index properties (modified from Pineda *et al*., 2016a): (a) natural water content, liquid limit and plastic limit; (b) dry density; (c) particle size distributions (PSD); (d) electrical conductivity (EC); (e) organic matter; (f) density of solids

water is generally saline. The conductivity reduces in the upper 3 m of the soil profile, which may indicate that some leaching has occurred, perhaps as a consequence of rain water. When sediment is dumped into salt water, the clay particles flocculate, causing them to settle with the silt and fine sand to form a loose porous fabric. Owing to the very low rate of sediment accumulation, marine clays typically display large and dense aggregates separated by large voids (Mitchell, 1976). This explains the large void ratios reported by Pineda *et al*. (2016a) for the natural clay (~ 3).

The depositional history suggests that the ground is likely to be geologically normally consolidated, as substantial

Table 1. Summary of geological units

Thickness: m	Description	CT scans borehole Inclo 2 (depth: m)	Stratigraphy
0·2 to 0·4	Organic material derived from sugar cane. Black, high plasticity with many roots present, very soft when wet, stiff when dry	0–0·5 	Topsoil
1·1 to 1·3	Clayey, sandy silt/clayey, silty sand. Brown, low-plasticity silt with roots present, fine to medium grained sand, stiff	0·5–1·0 	Alluvium
8·5 to 21 increasing in thickness towards the east	Silty clay. High plasticity, dark grey, some shells particularly concentrated at about 3·5 m depth. Occasional calcium nodules. Very soft at about 1·5 m depth and linearly increasing in strength with depth	2·1–2·7 3·3–3·9 7·5–8·1 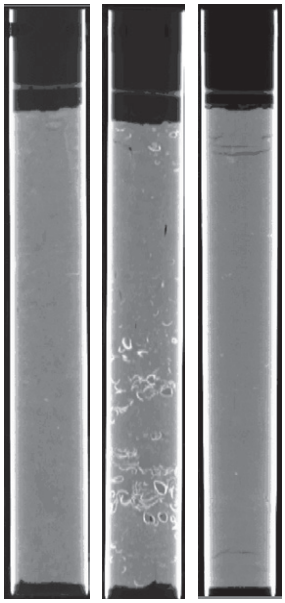	Estuarine (Ballina Clay)

Continued

Table 1. *Continued*

Thickness: m	Description	CT scans borehole Inclo 2 (depth: m)	Stratigraphy
1·0 to 2·0	Sand fining upwards to clay. Grey, fine-grained sand. Occasional stiff clay and timber fragments near the base of the layer	11·1–11·7 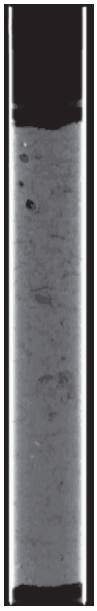	Transition zone
1·0 to 9·0	Sand, grey, brown and white layers, fine grained, medium dense to dense		Holocene sand
13 to 15	Silty clay, high plasticity, grey and green-grey, stiff to hard		Pleistocene clay
	Argillite meta-sediments encountered at a depth of about 38 m		Bedrock

erosion is unlikely to have occurred. Overconsolidation through seasonal changes in groundwater levels, creep or thixotropy may have occurred.

LABORATORY CHARACTERISATION

A comprehensive experimental programme was carried out to characterise the deposits that constitute the soil profile at the Ballina site. This included the determination of index and mechanical properties on specimens obtained from a borehole drilled for installation of an inclinometer (Inclo 2) prior to construction of an adjacent trial embankment and a second borehole drilled for an extensometer (Mex 9) used in a second embankment constructed without vertical drains (see Fig. 1(b)). Laboratory tests were performed on high-quality tube specimens retrieved with an Osterberg-type fixed-piston sampler (89 mm in external diameter and 600 mm effective length). Tubes were scanned prior to testing to assess the sample quality and to select specimens for mechanical tests. Detailed description of the laboratory characterisation is given in a companion paper by Pineda *et al.* (2016a).

A preliminary characterisation of the soil profile was obtained from the visual inspection of the materials encountered during borehole drilling. This is summarised in Table 1, where seven geological units are distinguished. The estuarine soft clay deposits (Ballina clay) lie below organic topsoil and alluvial deposits. Roots are frequently observed at shallow depths (typically above 3 m). These are indicated by black cavities in Table 1. The Ballina clay overlies a transition zone composed of clayey/silty sands as well as a thick layer of Holocene sand. Deeper units correspond to Pleistocene clays and the bedrock. Inspection of computer tomography (CT) scans included in Table 1 clearly shows the presence of a shelly zone in the estuarine clay (represented as white inclusions) located at around 3·3–4·0 m depth. This may be a transition between two depositional environments as discussed in the geological model by Bishop (2004).

Figure 2 shows the results of the classification and index tests performed on the alluvium and Ballina clay. The Ballina clay has a clay content ranging from 60% to 80% by size, an organic content of 1% to 3% by mass, a liquid limit (fall cone test) ranging from 80% to 130%, a moisture content slightly lower than the liquid limit and a plastic limit ranging from 40% to 50%. The minimum dry density is about 0·65 Mg/m^3, which corresponds to a void ratio of about 3.

The fabric of the natural Ballina clay has been recently studied by means of microscope images obtained from scanning electron microscope (SEM) images on high-quality block specimens retrieved with the Sherbrooke sampler (Pineda *et al.*, 2016b). As observed in Fig. 3 the structural arrangement of the natural clay shows an open configuration with no preferential orientation. This behaviour is in agreement with the non-oriented fabric of soft marine illitic clays described by Mitchell (1976). Macro-voids of around 1–2 μm size are detected, which is consistent with the dominant pore diameter detected from mercury intrusion porosimetry (MIP) tests for the natural clay (Pineda *et al.*, 2016b).

Mechanical parameters were estimated from oedometer and triaxial tests (Pineda *et al.*, 2016a). Values of yield stress, yield stress ratio, shear wave velocity at in situ stress (using bender elements), vertical consolidation coefficient and water permeability were estimated from constant rate of strain (CRS) tests, whereas the creep behaviour was evaluated from

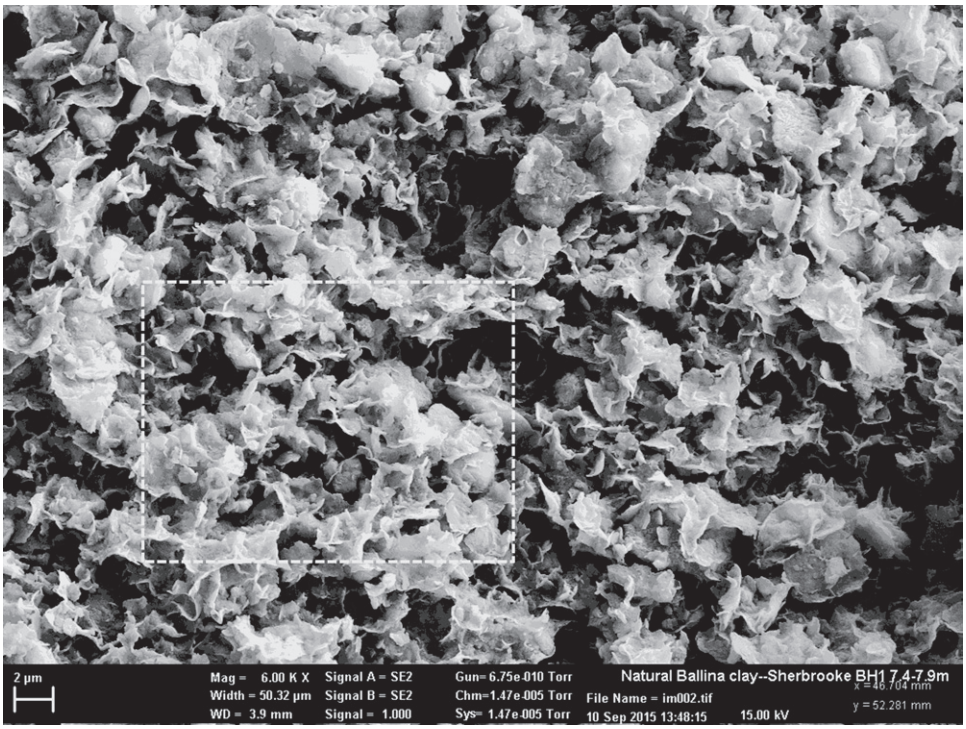

(a)

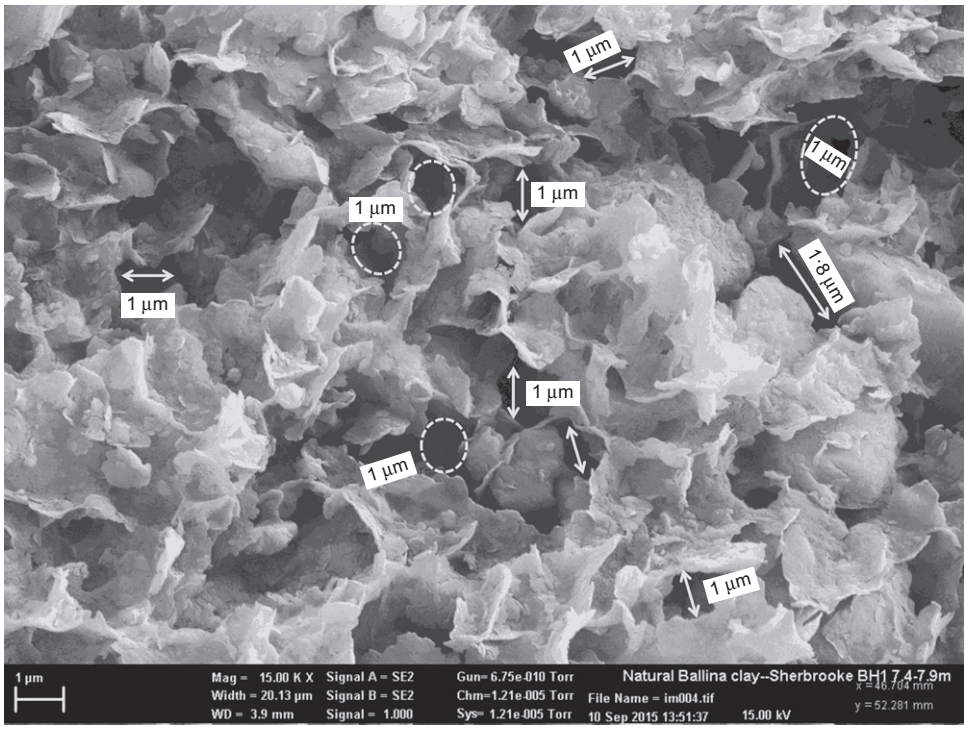

(b)

Fig. 3. Structural arrangement for intact Ballina clay ($z \approx 7{\cdot}5$ m): (a) large-scale view of soil fabric; (b) small-scale view of soil fabric

incremental loading (IL) tests. The undrained shear strength was estimated from triaxial tests (compression and extension) carried out on specimens anisotropically consolidated (recompressed) to their in situ stress state prior to undrained shearing. Values of vertical effective stress (σ'_{v0}) and coefficient of lateral earth pressure (K_0) applied during triaxial testing were obtained from laboratory estimations of bulk density and readings of groundwater levels at the time of sampling and the first in situ campaign (CPTu and SDMT data). The profiles of the mechanical parameters with depth for Ballina clay are shown in Fig. 4. Very good agreement is observed between the in situ shear wave velocity, obtained from seismic dilatometer tests at locations SDMT1 and SDMT34, and bender element measurements during CRS loading at in situ stress levels. This confirms the good quality of the specimens used for laboratory testing. A quasi-linear variation of the undrained shear strength (s_u) and the yield stress ratio (YSR) with depth is observed. It is important to note that values of the yield stress shown in Fig. 4 have not been corrected for strain rate effects. The minimum value of the YSR is about 1·6 and the difference between the yield stress and the effective stress is about 30 kPa. Some of the difference may be

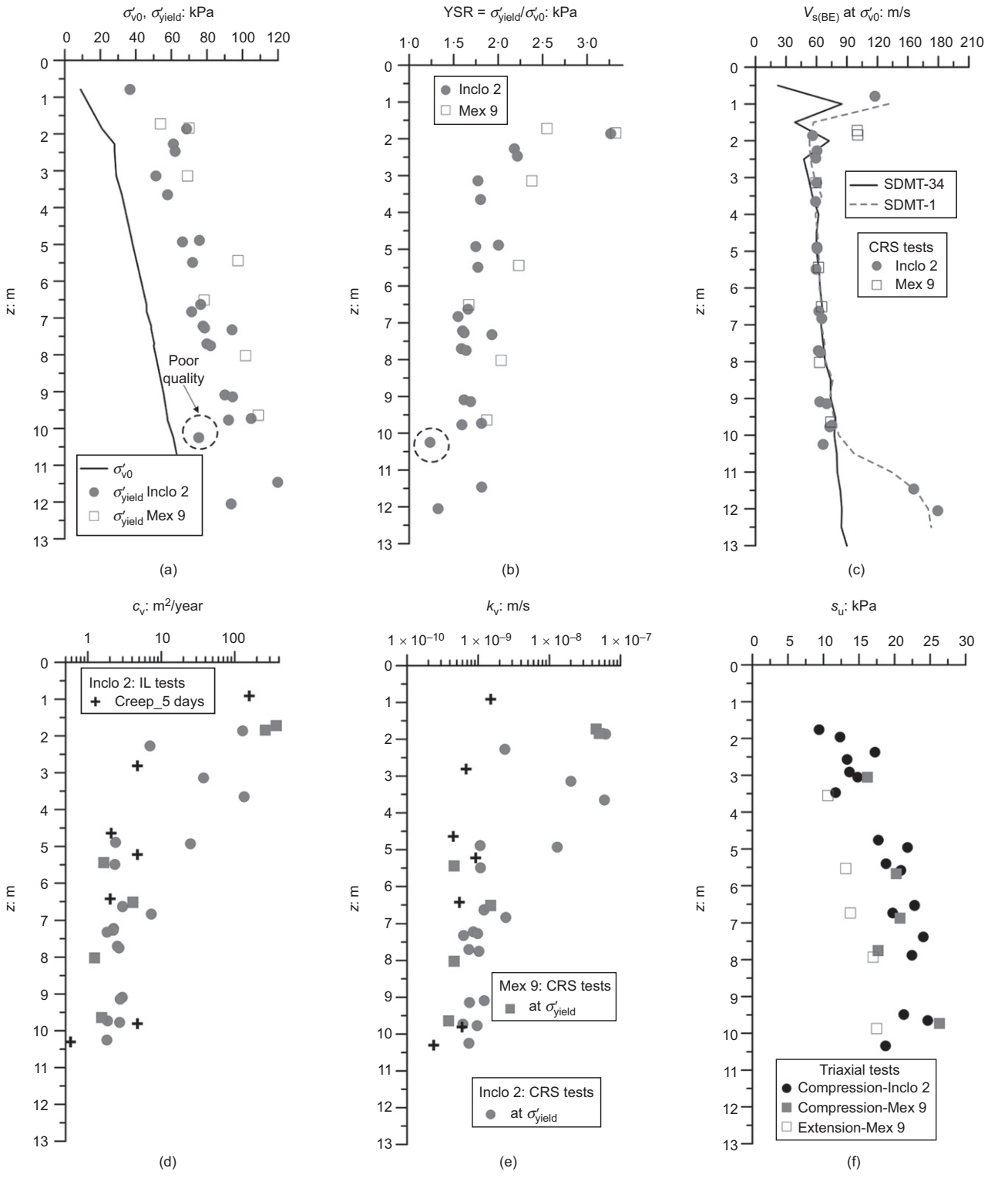

Fig. 4. Mechanical properties obtained from laboratory tests (modified from Pineda *et al.*, 2016a): (a) the variation of σ'_{yield} with depth; (b) the variation of YSR with depth; (c) variation of shear wave velocity with depth; (d) variation of coefficient of vertical consolidation with depth; (e) variation of permeability with depth; (f) variation of undrained shear strength with depth

attributed to changes in the groundwater level, whereas the remaining increment of yield stress is attributed to other mechanisms such as creep and thixotropy. The coefficient of vertical consolidation ranges from 1 m^2/year to 10 m^2/year and the permeability ranges from 10^{-10} m/s to 10^{-9} m/s. Inspection of Figs 2 and 4 shows small variation of the index and mechanical properties below 3·3–4·0 m depth (borehole Inclo 2), which corresponds to the estuarine soft clay deposits underlying the shelly zone shown in Table 1.

SITE STRATIGRAPHY

The stratigraphy across the site has been assessed by combining data collected from electrical resistivity imaging (ERI) geophysics (Burger, 1992) and multi-channel analysis of surface wave (MASW) geophysics (Foti *et al.*, 2015) with in situ tests and boreholes. The ERI electrode spacing was 2 m, whereas the MASW spacing was 5 m. Both the ERI and MASW measure signals at the ground surface, which are then subjected to mathematical inversion to

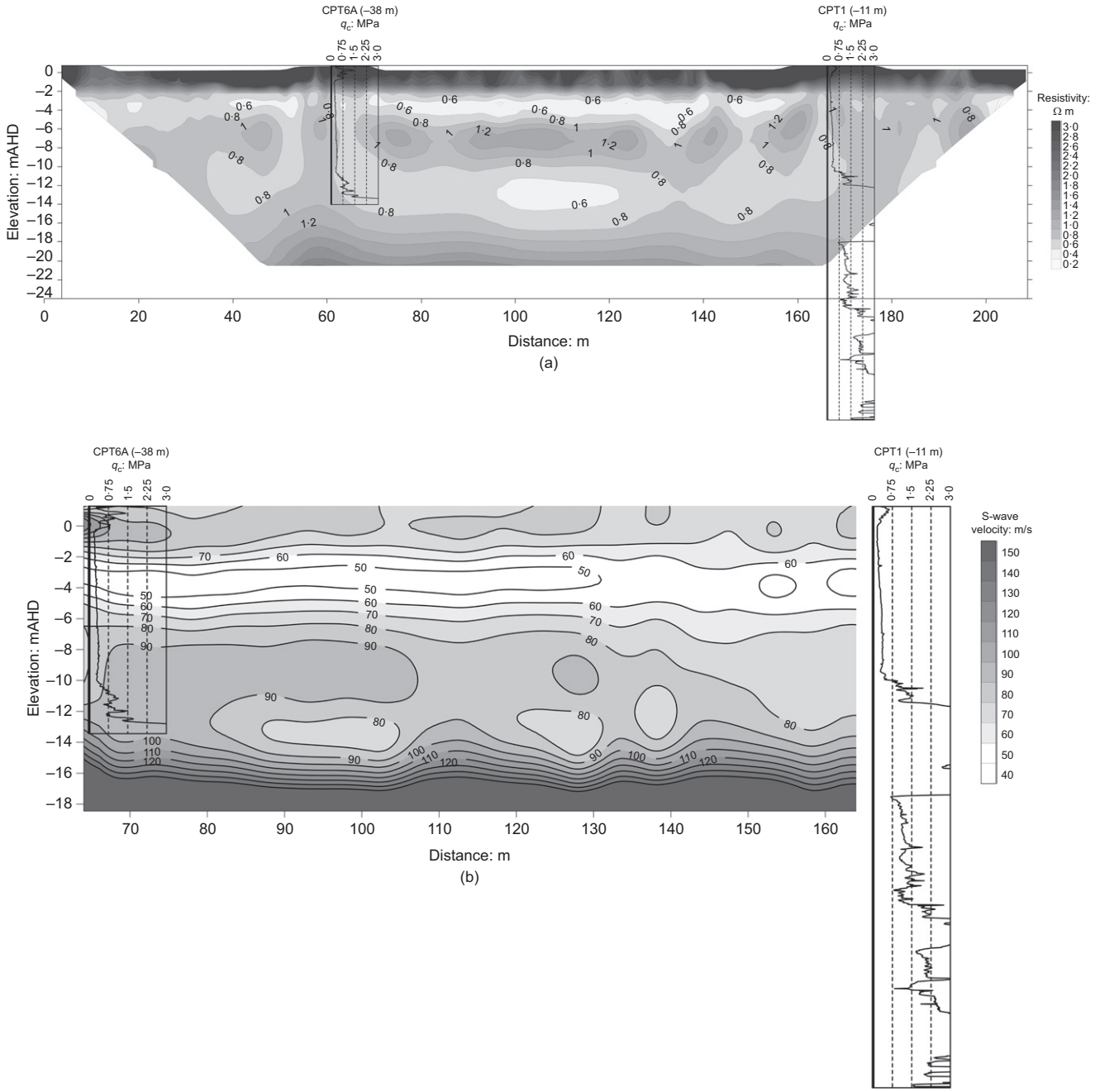

Fig. 5. (a) ERI2 and (b) MASW2 geophysics along north–south direction

provide profiles of resistivity and shear wave velocity with depth. The resolution of the subsurface profiles depends on the spacing of the surface instruments and the inversion process and is in the order of 1 m. Despite this relatively low resolution, both techniques broadly capture the stratigraphic boundaries. Resistivity and shear wave velocity profiles obtained along north–south and east–west sections, together with the cone penetration test (CPT) cone resistance plots, are shown in Figs 5 and 6, respectively. The geophysical data show the spatial extent of the geological units described previously in Table 1. The results show that the stratigraphy comprises the alluvial crust which is underlain by the Ballina clay, a transition zone with increasing sand content, sand and stiff clay. The various layers are relatively uniform with depth along the north–south direction. In contrast, the thickness of the soft clay layer increases towards the east, whereas the sand layer decreases in thickness. The ERI clearly picks up the boundary between the crust and the soft clay as well as the boundary between the sand and the stiff clay; however, the boundary between the soft clay and the sand is less well defined. The MASW defines the boundary between the soft clay and sand at a shear wave velocity between about 80 m/s and 100 m/s in the north–south direction and between about 90 m/s and 100 m/s in the east–west direction. Resistivity values are low, which is indicative of a highly conductive medium such as saline groundwater.

The CPT data define the stratigraphic boundaries clearly and consistently across the site due to the high density of measurements in the vertical direction. The CPT data appear to indicate consistent stratigraphy in the horizontal direction, albeit for widely spaced tests. The close spacing of the ERI and MASW data provides an advantage over the CPT tests in that it has the potential to detect subsurface features such as palaeochannels that might have been missed by penetrometry and borehole drilling. In this case, the geophysics has not

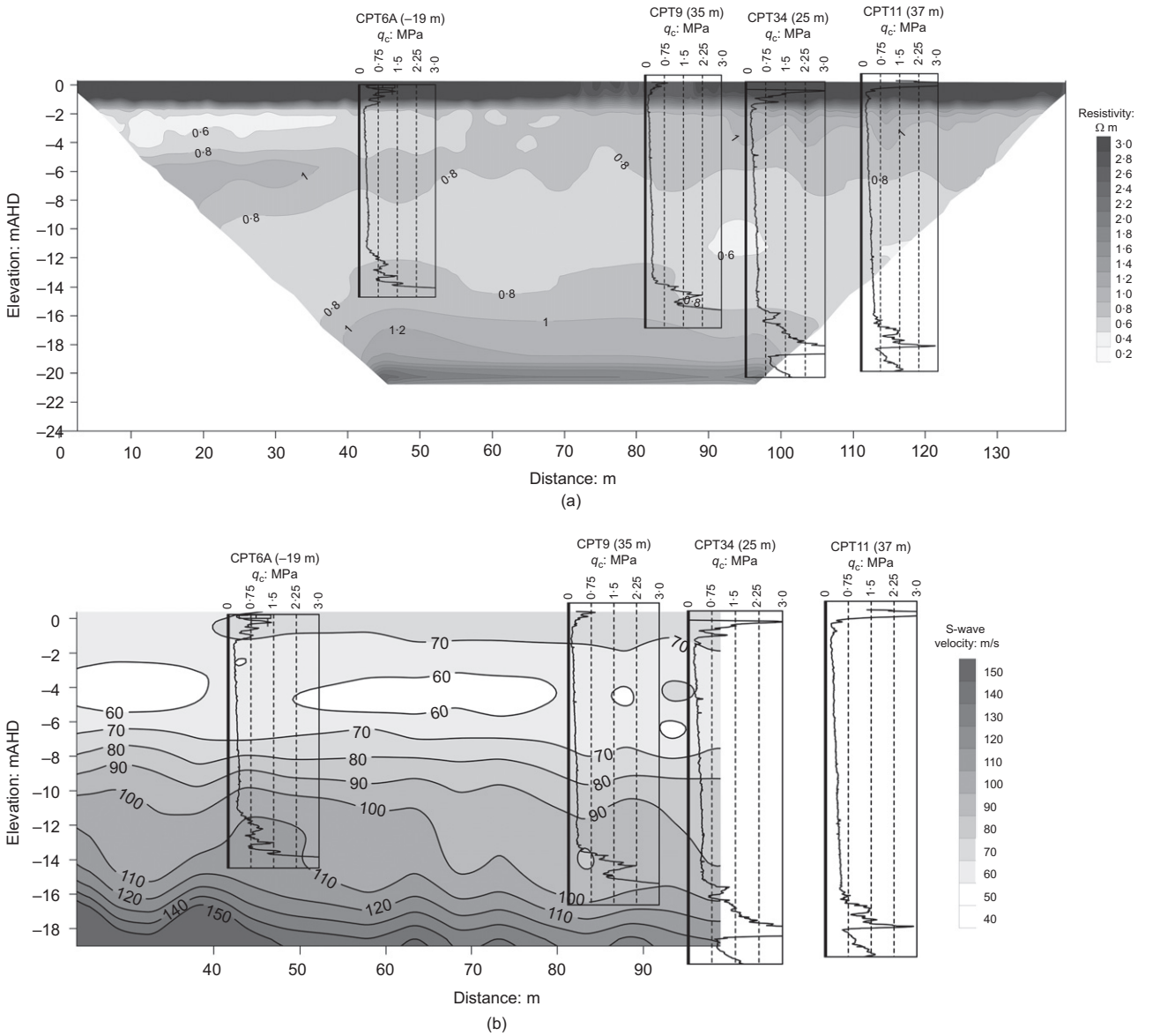

Fig. 6. ERI and MASW geophysics along east–west direction

detected any significant subsurface features within the footprint of the tests.

GROUNDWATER

Data obtained from vibrating wire piezometers (VWPs) installed within the Ballina clay below the footprint of the western embankment (i.e. with vertical drains) show that the groundwater is hydrostatic (see Fig. 7(a)). Fluctuations in groundwater levels have been inferred from pore pressure readings taken by push-in pressure cell PIPC12 (see Fig. 1(b)). The ground level at this location lies at RL0·46 mAHD and the PIPC pore pressure filter lies at 4·35 m depth. The temporal variation of the water level is shown in Fig. 7(b). There, daily rainfall observations from the nearby Ballina airport have also been plotted. The water level when readings began on 16 August 2013 was about RL−0·3 mAHD and fluctuated between roughly RL−1·0 mAHD and RL+1·0 mAHD. This fluctuation implies that the groundwater level can reduce to the base of the upper clayey sandy silt layer and rise to 0·5 m above ground level. Groundwater can lie above ground level due to standing water after heavy rainfall. The fluctuation in groundwater level causes seasonal changes in mean effective stress in the soil in the order of 15 kPa at a depth of 4·35 m. Variations in groundwater at greater depths are expected to be smaller than shown in Fig. 7(b) due to the reduction in soil permeability. The PIPC installed at greater depths became unreliable within a few weeks post-installation and a long-term trend of pressures at depth is not available. In Fig. 7(c), a groundwater depth of 0·3 m (RL 0·15 m AHD) was estimated from the U2 data from cone penetrometer CPT7 by comparing the hydrostatic line to the U2 pressure measured in the sand layer between 14 m and 18 m depth. The CPT7 was performed on 12 June 2013 before PIPC was installed, but the groundwater level inferred from CPT7 appears to be consistent with the water levels inferred from the PIPC for similar rainfall patterns. Groundwater levels at most locations were inferred from the CPTs.

PARAMETER CHARACTERISATION USING IN SITU TESTS

Strength, stiffness and permeability parameters for the Ballina clay have been derived by way of the laboratory testing programme at specific locations at the site. In order to estimate what the mechanical parameters are at locations

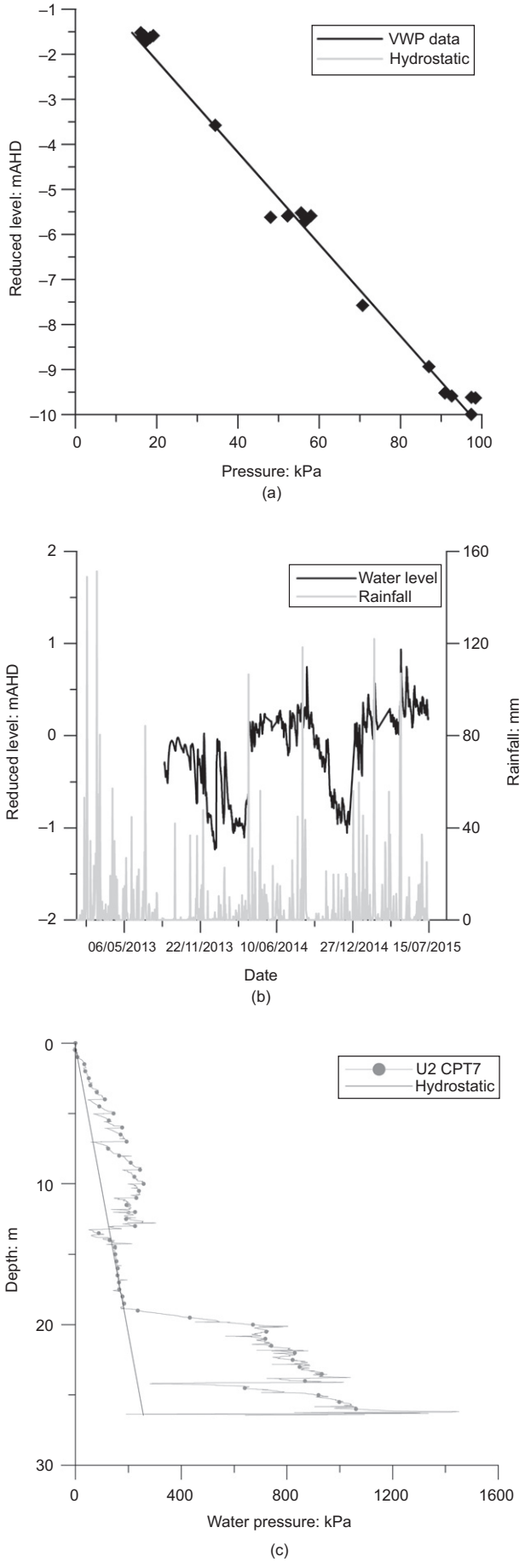

Fig. 7. (a) Vibrating wire piezometer data. (b) Water level observed in PIPC12 at 4·3 m and rainfall at Ballina Airport. (c) Water pressure (U_2) observed in CPT7

elsewhere in the site (or geological deposit) it is conventional to perform a high number of in situ tests relative to laboratory tests and calibrate the two data sets in order to characterise a large volume of ground rapidly and economically. Comparisons between interpretation of the in situ tests and the laboratory test data are made in the following sections.

The primary data from CPTu and SDMT tests are summarised in Figs 8 and 9. The CPTu was calibrated in a pressure chamber to obtain the cone tip area ratio, which was found to be 0·76. The area ratio of the sleeve was found to be zero.

Soil behaviour type (SBT) has been assessed from CPTu data using the Robertson (1990) charts, presented in Fig. 10. In Fig. 10, Q_{tn}, F_R and B_q are the normalised cone resistance, normalised friction ratio and normalised pore pressure defined by Robertson (1990). The interpretation is generally consistent with the gradings obtained from laboratory tests (Fig. 2), except between 11 m and 12 m depth where the piezocone interpretation suggests clay and the laboratory tests describe a silty sand.

Methods of interpretation adopted for the in situ tests are summarised in Table 2. Parameter descriptions are provided in the notation list.

In situ stresses

Bulk unit weights were calculated from moisture content and specific weight of solids measurements reported by Pineda *et al.* (2016a) and these data were then used to estimate the total vertical stress with depth. Effective vertical stresses were computed by subtracting the hydrostatic pressure from the total stress. Total stresses, hydrostatic water pressures and effective stresses calculated at the location of cone penetration test CPT6 are shown in Fig. 11.

Horizontal earth pressures and associated K_0 values are difficult to determine in the laboratory and have been assessed using in situ methods. Total horizontal pressure and water pressure were measured using three PIPCs, and these were used to estimate the effective horizontal pressure and coefficient of lateral earth pressure (K_0). The PIPCs were installed at 4·35 m, 8·4 m and 12·6 m depths. The difference between the two measurements is inferred to be the effective horizontal stress. Measurements of total horizontal pressure in stiff clays are conventionally corrected to account for disturbance during installation. However, installation effects do not appear to be as significant in soft clays (Richards *et al.*, 2007) and no correction to the data has been made.

Values of K_0 have also been estimated using the SDMT and CPTu. The SDMT has been interpreted using Marchetti (1980), Powell & Uglow (1988) and Kouretzis *et al.* (2015). Profiles of the K_0 estimated from dilatometer test SDMT1 are shown in Fig. 11(c) and are compared with the PIPC data ($K_0 = 0{\cdot}54$, 0·46 and 0·16 at RLs of −3·89 mAHD, −7·88 mAHD and −12·09 mAHD, respectively). The interpretation of Kouretzis *et al.* (2015) is closest to the PIPC data, while Powell & Uglow (1988) and Marchetti (1980) are 28% and 70% higher than Kouretzis *et al.* (2015), respectively. The Marchetti (1980) interpretation has been shown by Lacasse & Lunne (1988), Powell & Uglow (1988) and Cao *et al.* (2015) to overestimate field measurements in soft clays. The numerical results of Kouretzis *et al.* (2015) indicate that all of these methods overestimate K_0 when the K_D value lies approximately between 2 and 7 for the parameters and model adopted in their study.

Results from CPTu tests have been used to compute values of K_0 according to the expression (Kulhawy &

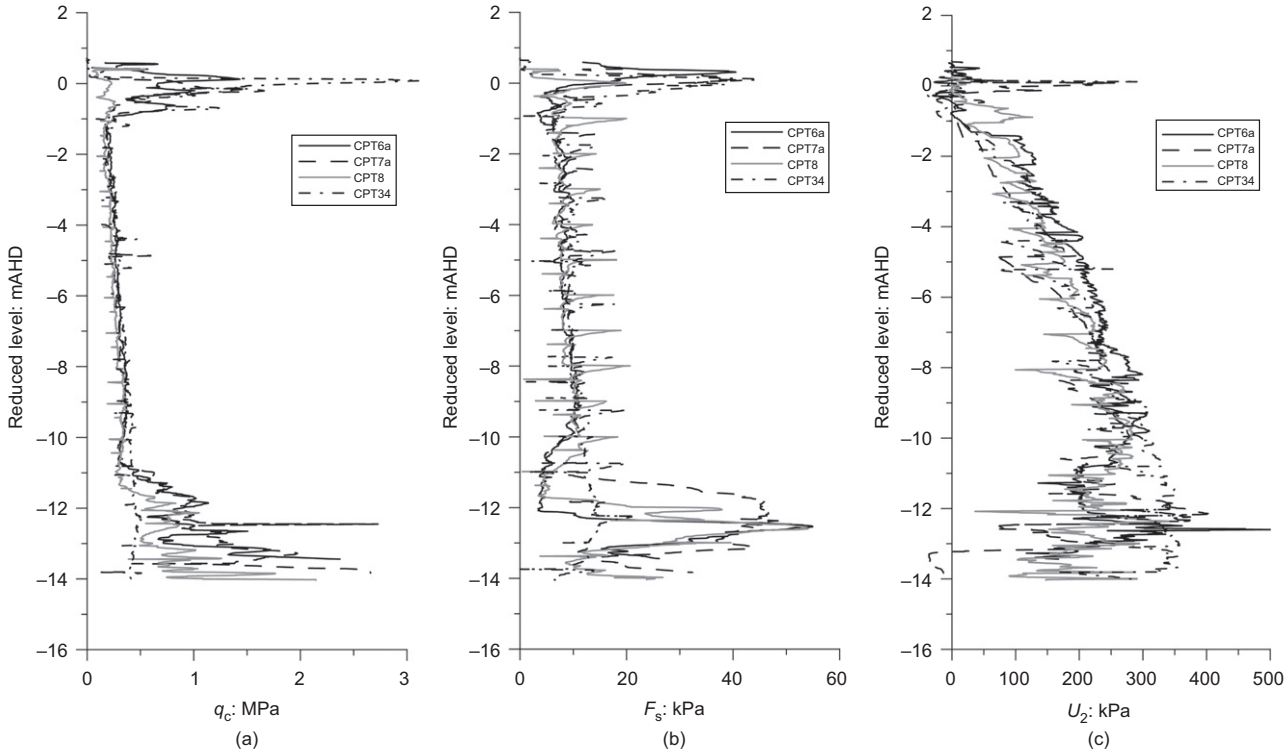

Fig. 8. (a) Cone tip resistance. (b) Sleeve friction. (c) Water pressure (U_2)

Mayne, 1990)

$$K_0 = (1 - \sin\phi)\mathrm{OCR}^{(\sin\phi)} \quad (1)$$

This approach requires knowledge of the overconsolidation ratio (OCR) and friction angle (ϕ'), both of which can be estimated from CPTu data as discussed in the following sections on 'Friction angle' and 'Yield pressure'. For the purpose of this assessment, values of friction angle estimated from triaxial tests at deformations larger than 10% (associated here to constant volume friction angle) have been used in combination with yield pressures obtained from CRS compression tests. Values of yield pressure have been corrected in this calculation to account for rate effects as discussed by Pineda *et al.* (2016a). The comparison between K_0 values estimated from CPTu results and the PIPC data (Fig. 11(d)) shows that the CPTu interpretation provides slightly higher estimates of K_0 than the measurements. A slightly closer fit to the PIPC data can be obtained by using values of peak friction angle and non-corrected yield pressures.

The total horizontal pressure and pore pressure data from PIPC12 are shown in Fig. 12(a). An important aspect to remark is the potential seasonal fluctuation of K_0 due to variations in groundwater level. This phenomenon is illustrated in Fig. 12(b) where the temporal variations of K_0 at 4·35 m depth at PIPC12 are presented. The K_0 values have been calculated as the effective horizontal pressure measured by PIPC12 divided by an effective vertical stress calculated assuming that the bulk unit weight of the soil remains constant while the water level changes. The K_0 values calculated in this way vary from 0·4 to 0·65 as the water level changes over time. The implication of this behaviour is that an in situ test can only provide an estimate for K_0 at a particular instant. However, for the purpose of this assessment, average values of K_0 from the PIPC tests have been adopted. Pressure sensors PIPC10 (~12·6 m depth) and PIPC11 (~8·4 m depth) were only reliable for a short period of time after installation so that the average over that time has been adopted in this case. This effect will also reduce in magnitude with depth due to attenuation of water pressure changes.

It is interesting to note that the horizontal effective stress stays approximately constant as the water table varies. The variation of K_0 is mostly due to the change of vertical effective stress and this illustrates the variation of K_0 with OCR.

Friction angle

Mayne (2007) proposed a simplified expression for the methodology developed by Senneset *et al.* (1989) to estimate friction angles from CPTu data. The friction angle estimated in this way appears to represent a large strain parameter rather than a peak parameter (Mayne, personal communication, 2016).

Interpreted CPTu data (see Table 2) are compared with peak and large deformation (constant volume) friction angles obtained from CK_0U triaxial tests on natural and reconstituted samples in Fig. 13 and show that the CPTu interpretation is more similar to the constant volume friction angle data than to the peak friction angle. As observed in Table 2, a value of 29·5 is used for the determination of the friction angle following the approach of Mayne (1995, 2007). However, the best fit to the peak friction angle data reported here requires this quantity to be increased to 35·7.

Yield pressure, σ'_p

Results from CTPu and SDMT tests were used to derive profiles of yield pressure. In the CPT approach, an empirical constant is used to convert CPT data to yield pressure that typically ranges between 0·2 and 0·4 (given the value 0·33 in Table 2), q_t is the corrected cone tip resistance and σ_v is the total vertical stress. Estimation of the yield pressure from

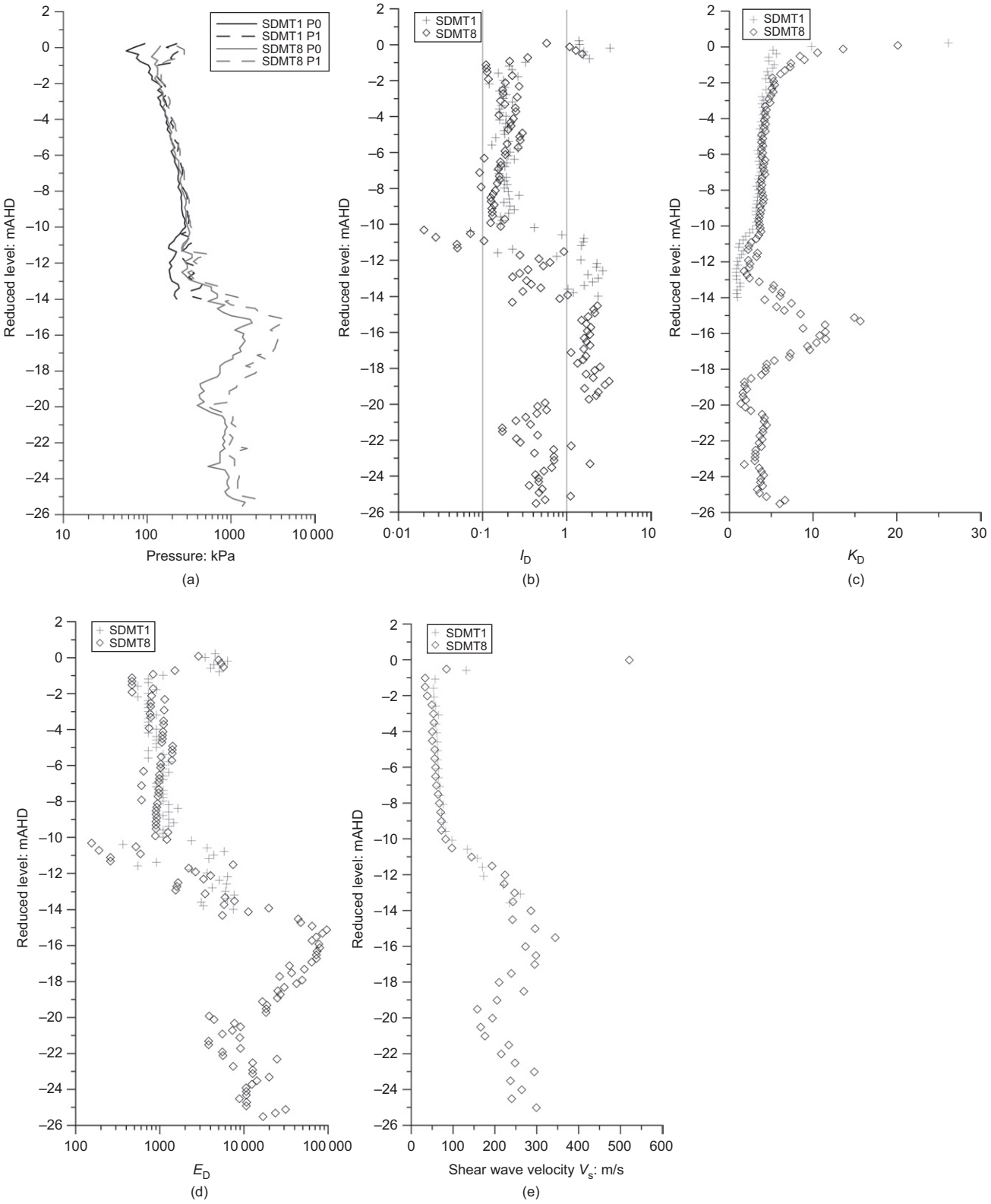

Fig. 9. (a) $P0$ and P_1 pressures. (b) Index I_D. (c) Index K_D. (d) Index E_D. (e) Shear wave velocity

SDMT data is based on the corrected first reading (P_0) and the equilibrium pore pressure (U_0) (Marchetti, 1980). Marchetti (1980), Powell & Uglow (1988) and Kouretzis *et al*. (2015) interpretations for OCR have been adopted and yield pressures obtained by multiplying by the in situ vertical effective stress. CPT and SDMT estimations have been compared with data obtained by Pineda *et al*. (2016a) from CRS compression tests estimated using the strain energy method proposed by Becker *et al*. (1987). The yield pressures used in this section are values interpreted from the CRS test data and were not adjusted for strain rate.

Figure 14(a) shows the comparison between in situ and laboratory data for yield pressure where a value of $k = 0{\cdot}34$ provides the best fit for the CPT expression (see Table 2). This value falls within the range reported by Lunne *et al*. (1997). Inspection of Fig. 14(a) shows a linear variation of yield

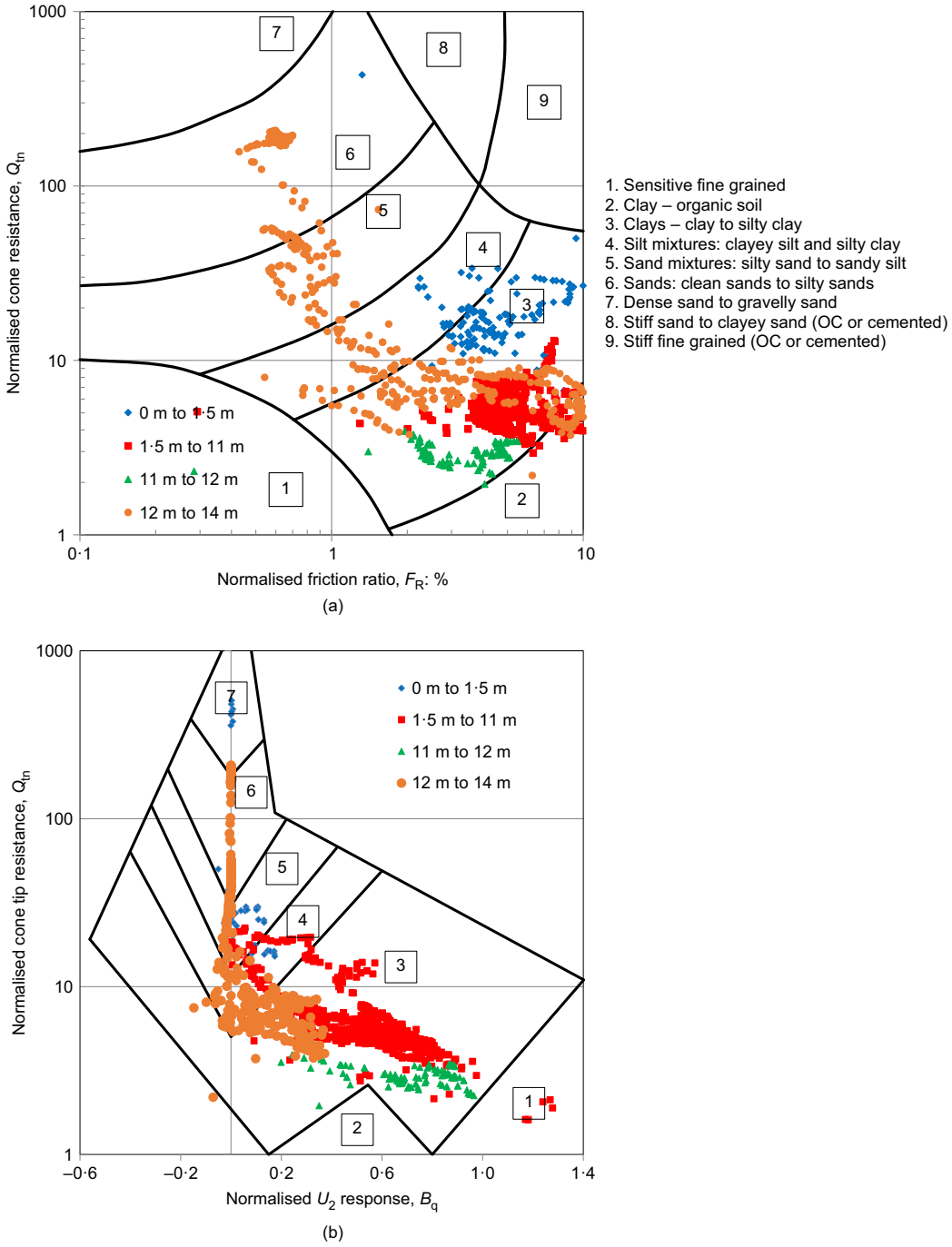

Fig. 10. (a) SBTn chart. (b) SBT B_q chart (Robertson, 1990)

pressure with depth between 1·5 m to 10 m depth, as would be expected in normally and slightly overconsolidated clays. The average yield pressure profile in this depth range is given by $\sigma'_p = 51 + 6{\cdot}7z$ (z in m), z being the depth below ground level. Interpretations from SDMT1 are shown in Fig. 14(b). The Kouretzis *et al*. (2015) and Powell & Uglow (1988) expressions are similar, but both methods underestimate the yield pressures. The Marchetti (1980) method provides estimates of yield pressure about twice the magnitude of the other methods and over-predicts the yield pressures. A good fit to the laboratory test data was obtained using Mayne (2007).

Undrained shear strength, s_u

Field vane tests were performed to estimate the variation of the undrained shear strength with depth. A 75 mm wide by 150 mm high by 2 mm thick AP van den Berg shear vane and a 65 mm wide by 130 mm high by 2 mm thick Geotech AB shear vane were used. The GeotechAB vane is initially retracted inside a housing and is pushed into the ground once the housing has been pushed to its target depth. Both shear vanes were pushed to the target depths from the ground surface, then rotated using electric heads and the torque was measured at truck level. The Geotech AB vane was rotated 15° prior to engaging with the vane in order to obtain an estimate of rod friction. The initial rate of shearing for both vanes was 0·15 to 0·2°/s. The rate of shearing was increased to 6°/s post-mobilisation of peak strength with the AP van den Berg vane for a distance equivalent to five rotations. The rate of shearing was increased to 1·5°/s for the Geotech AB vane for one complete rotation of the vane.

Peak and residual vane shear strengths from five test locations (DP2, DP6, SV7, SV8 and SV34) are plotted in

Table 2. Summary of equations

Parameters	In situ test	Equations	Reference
K_0	SDMT	$K_0 = 0{\cdot}36e^{0{\cdot}11K_D}$	Kouretzis *et al.* (2015)
		$K_0 = 0{\cdot}34(K_D)^{0{\cdot}55}$	Powell & Uglow (1988)
		$K_0 = \left(\frac{K_D}{1{\cdot}5}\right)^{0{\cdot}47} - 0{\cdot}6$	Marchetti (1980)
Yield pressure	CPTu	$\sigma'_p = 0{\cdot}33(q_t - \sigma_v)$	Mayne (2007)
	SDMT	$\sigma'_p = 0{\cdot}51(P_0 - U_0)$	Mayne (2007)
OCR	SDMT	$OCR = 0{\cdot}58e^{0{\cdot}23K_D}$	Kouretzis *et al.* (2015)
		$OCR = 0{\cdot}24(K_D)^{1{\cdot}32}$	Powell & Uglow (1988)
		$OCR = 0{\cdot}34(K_D)^{1{\cdot}56}$	Marchetti (1980)
s_u	CPT	$s_u = \left(\frac{q_t - \sigma_v}{N_{kt}}\right)$ $N_{kt} = 12{\cdot}2$ (triaxial) $N_{kt} = 13{\cdot}2$ (shear vane)	Values of N_{kt}
	SDMT	$s_u = f\sigma'_v OCR^x$ $x = 0{\cdot}8$: $f = 0{\cdot}22$	Marchetti (1980)
Peak friction angle	CPT	$\phi \approx 29{\cdot}5\left[B_q^{0{\cdot}121}\left(0{\cdot}256 + 0{\cdot}336B_q + \log Q\right)\right]$	Mayne (2007)
Permeability	BAT	$k_h = \frac{P_0 V_0}{Ft}\left[\frac{1}{P_0 U_0} - \frac{1}{P_t U_0} + \frac{1}{U_0^2} \times \ln\left(\frac{P_0 - U_0}{P_0}\frac{P_t}{P_t - U_0}\right)\right]$	Torstensson (1984)

Fig. 15. Test results are plotted as a single series, as no discernible difference between vanes is observed. The peak strength values show the alluvial crust has a soft to firm consistency, whereas the Ballina clay is generally soft with a linearly increasing strength given by: 12·5 kPa + 0·8z for depths (z) below 1·5 m. The residual undrained strength shows a linear increase with depth given by: 4·3 kPa + 0·3z. The sensitivity, defined as the peak vane shear strength divided by the residual vane shear strength, is plotted in Fig. 15(b) and shows that the sensitivity ranges between 1·5 and 5·5, but is generally about 2 to 4. There is an increase in sensitivity in the upper alluvial layer and some outliers at depth in the transition zone. A comparison of peak undrained strengths from vane tests and triaxial compression and extension tests (Fig. 4(f)) shows that, as would be expected, s_u is greatest in triaxial compression, intermediate in vane shear and least in triaxial extension. The variations with depth are 8·4 kPa + 2z for depths between 1·5 m and 8 m for triaxial compression and 10·7 kPa + 1·2z ($3{\cdot}5 < z < 10$ m) for triaxial extension.

The CPTu and SDMT data were compared with shear vane and triaxial compression test results. The comparison between CPTu and SDMT estimations against vane shear and triaxial results shows a similar trend, as observed in Fig. 16. Values of N_{KT} obtained for assessing shear vane and triaxial tests are equal to 13·2 and 12·2, respectively. The different values are attributed here to two factors: (*a*) the differences in the shear mode involved in each test, and (*b*) the differences in strain rate between tests (triaxial specimens were sheared using a strain rate of 5%/day). Similar findings have been reported by Low *et al.* (2011) whose estimated mean values for N_{KT} were 14 and 11·3 after correlating CPT data with, respectively, field vane shear and triaxial compression tests on Burswood clay. Values of N_{KT} reported here are also consistent with the range reported by Randolph (2004) derived from theoretical analysis ($10{\cdot}2 < N_{KT} < 13{\cdot}9$).

Interpretation of s_u from SDMT tests requires an indirect approach where OCR, the ratio of undrained shear strength to effective vertical stress for a normally consolidated soil (f in Table 2) and an exponent (x in Table 2) must be first determined. The values adopted by Marchetti (1980) cause the SDMT data to fit well with triaxial and shear vane test data in Fig. 16(b). Adoption of $f = 0{\cdot}22$ and $x = 0{\cdot}8$ appears to compensate for the over-prediction of yield pressures using Marchetti (1980).

CONSOLIDATION COEFFICIENTS AND PERMEABILITY

Coefficients of horizontal consolidation (c_h) and vertical consolidation (c_v) have been interpreted from the results of CPTu dissipation testing and compared against values from CRS tests. Interpretation of the dissipation tests has been performed using a curve fit to Teh & Houlsby (1991) method provided by Mayne (personal communication, 2006). Interpretation of the dissipation test requires an assessment of the rigidity index (I_R) of the soil, which was estimated from the CK_0U triaxial tests reported by Pineda *et al.* (2016a) as $I_R = G_{50}/s_u$. A value of I_R equal to 85 was estimated between RL−2 m and RL−7 m, whereas an I_R of 125 was adopted below RL−7 m. These values are consistent with typical values for near normally consolidated clays with plasticity index, PI > 50% (Duncan & Buchignani, 1976). Finally, the coefficient of horizontal consolidation, c_h, was estimated from the comparison between measured and theoretical dissipation curves. An example of the curve fit is provided in Fig. 17 where the curve has been fitted to the tail of the dissipation curve to overcome the initial rise in measured pore pressure described above.

Figure 18(a) shows a comparison of c_h values from CPTu and piezoball (Colreavy *et al.*, 2016) dissipation tests with c_v values estimated from CRS tests at yield stress. Very good agreement is observed between laboratory and the dissipation test results. For the materials from RL 2 to RL 10 m, $c_{v\text{-yield}}$ lie between 2 and 10 m^2/year whereas the c_h varies from 1·5 to 15 m^2/year. Horizontal (k_h) permeability has been obtained from BAT tests (Torstensson, 1984). A detailed description of the equipment and procedure is provided by BAT GMS (2016). Values of k_h were estimated using the

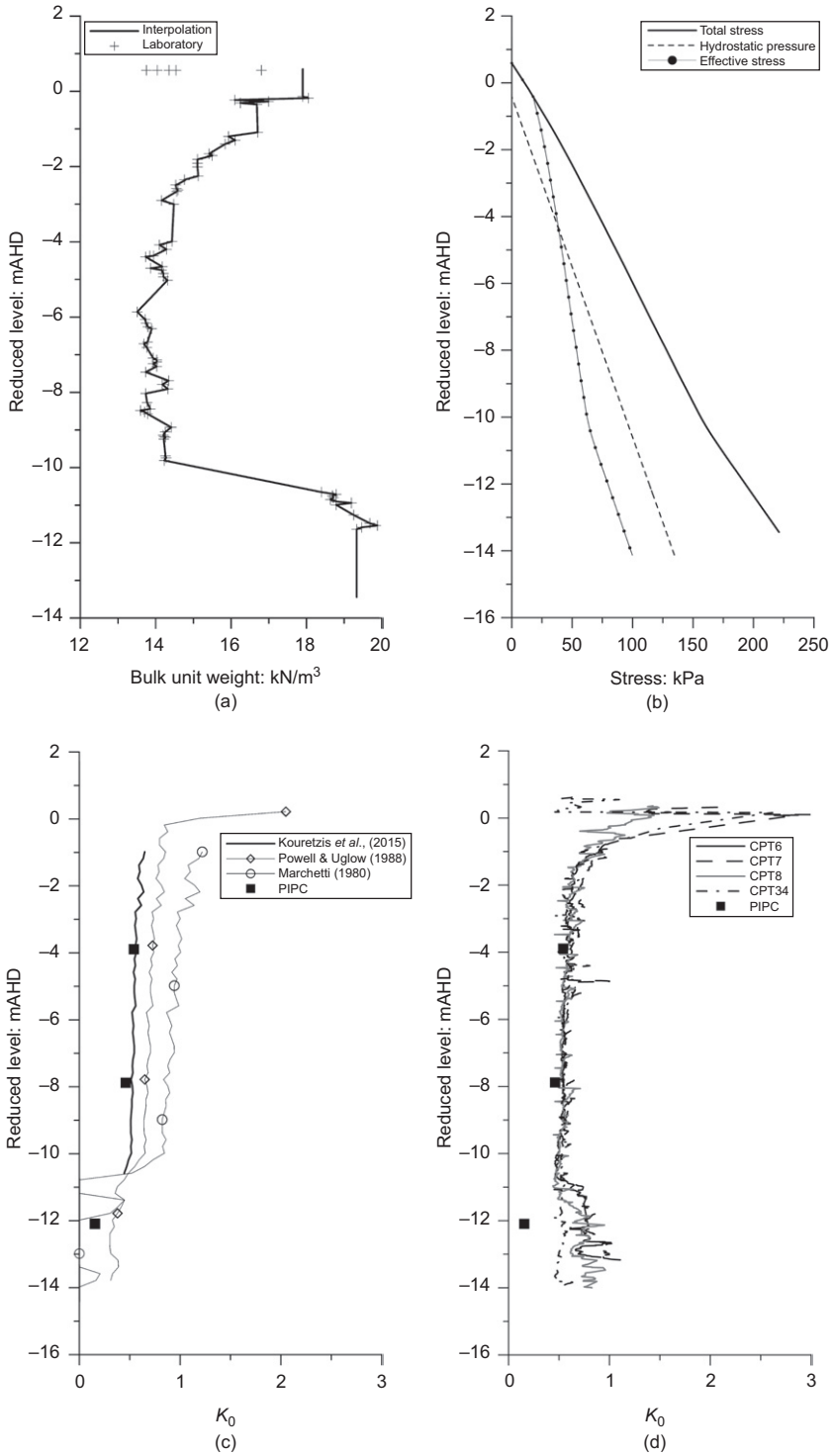

Fig. 11. (a) Bulk unit weight. (b) Total vertical stress, hydrostatic water pressure and effective vertical stresses CPT6. (c) K_0 from SDMT tests. (d) K_0 from CPT tests

expression given in Table 2. There, P_0 is the initial system pressure, V_0 is the initial gas volume, P_t is the pressure at time t, F is the shape factor and U_0 is the static pore pressure. For the tests carried out on Ballina clay, F was assumed equal to 230 mm.

Figure 18(b) compares the horizontal and vertical water permeability obtained from BAT and CRS tests, respectively. Despite the few data obtained from BAT tests, there is a good agreement between in situ and laboratory data. The small differences between c_h and c_v as well as k_h and k_v suggest a low permeability anisotropy for Ballina clay, as is also recognised by Leroueil *et al.* (1990) for homogeneous marine clays. It would be consistent with the non-oriented structural arrangement observed from scanning electron microscopy (SEM) analysis (Fig. 3). However, further data are required to confirm this feature in natural Ballina clay.

DISCUSSION

The hypothesis that sediments were generated by chemical weathering of rocks then deposited in low-energy estuarine conditions, deposited under salt water, appears to be

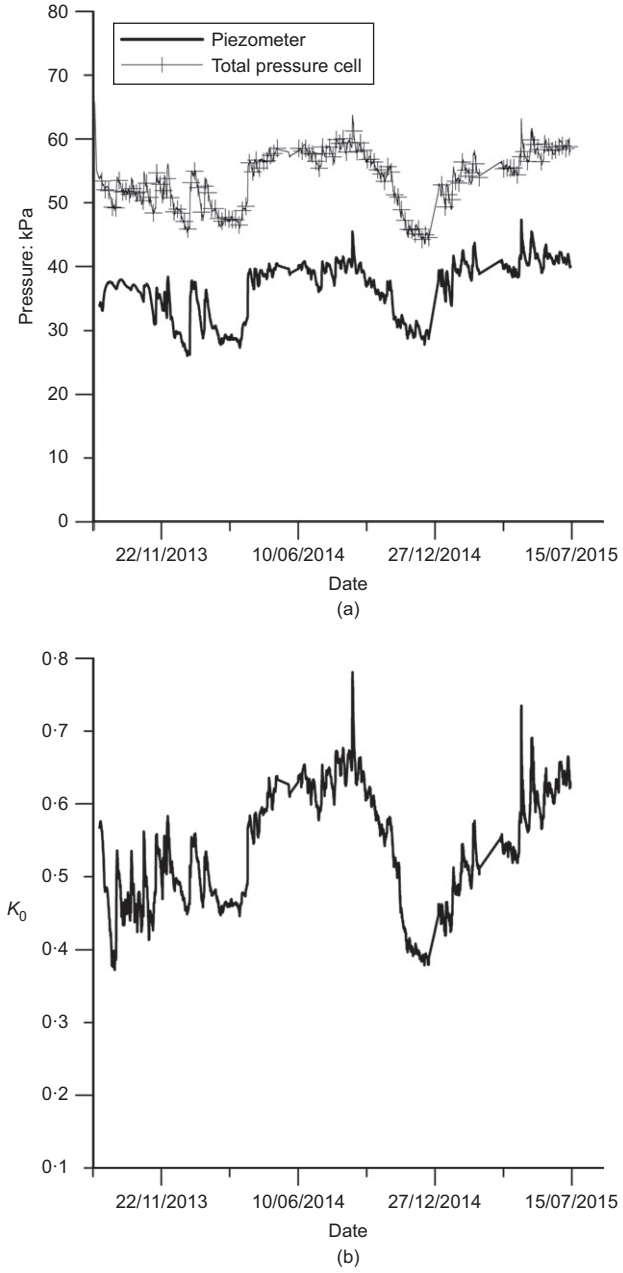

Fig. 12. (a) Pressure data. (b) Variation in K_0 with time at PIPC12 at 4·35 m depth

supported by the SEM images, mineralogy and conductivity tests. Clays deposited under these conditions would be expected to have a relatively uniform structure over large distances. The saline depositional conditions have created a soil with sensitivity between 2 and 6. For Norwegian clays, the sensitivity ranges from 4 to 6 at a salt concentration of 30 g/l to greater than 100 at a salt concentration of 5 g/l (Bjerrum, 1954). The electrical conductivity measurements on pore water are consistent with a salt concentration ranging from 20 to 35 g/l and therefore the sensitivity of the Ballina clay is consistent with Norwegian clays at a similar salinity. The clay displays an open flocculated structure so that high compressibility and low strength would be expected. The uniformity of the soil profile at the Ballina site has been recently confirmed through a statistical analysis of 26 CPT test data aimed at predicting the stratigraphy at locations away from measurements (Li *et al.*, 2016). The results showed that the correlation distance in the horizontal direction ranges between 40 m and 60 m.

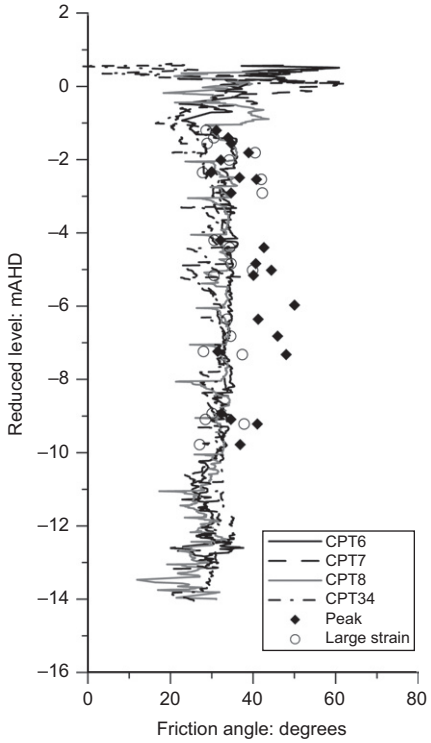

Fig. 13. Estimation of the peak friction angle from in situ tests

According to Burland (1990), the state and structure of soil can be assessed by comparing its natural state against the reference properties of the reconstituted material. It can be conveniently evaluated by using the void index concept (Burland, 1990) $I_v = (e - e^*_{100})/C^*_c$, which requires the determination of two parameters, e^*_{100} and C^*_c, that represent the compressibility of the intrinsic material. Fig. 19(a) shows values of in situ void index (I_{v0}) against the in situ vertical stress (σ'_{v0}) for specimens from borehole Inclo 2. The intrinsic compression line (ICL) and the sedimentary compression line (SCL), determined by the Burland (1990) approach, are included as a point of reference. The pairs of I_{v0}–log σ'_{v0} all lie above the ICL, which is indicative of the natural structure of the clay. Pineda *et al.* (2016a) showed that important destructuration takes place during one-dimensional loading as the stress level increases beyond the yield stress, σ'_{yield}, leading the compressibility curves to converge to the ICL. A similar assessment can be done by plotting the in situ liquidity index (LI) against the in situ vertical stress, σ'_{v0} (see Fig. 19(b)), which provides an indication of the soil fabric sensitivity. Figure 19(b) includes data for European clays reported by Skempton & Northey (1953), as well as the theoretical expression for the variation of LI plotted against σ'_{v0} (grey dashed lines) proposed by Muir Wood (1990). The in situ stress state for Ballina clay falls in between lines for $k = 0$ and $k = 2$, which indicates soil sensitivities (at water contents equal to the liquid limit) ranging between 2 and 8 (Muir Wood, 1990).

Soil anisotropy is, however, not only reflected by the structural arrangement of the soil fabric. Different degrees of soil anisotropy may be observed in terms of strength and permeability. A low level of anisotropy is indicated by the similarity between the magnitudes of coefficients of vertical consolidation in CRS tests and horizontal consolidation inferred from CPTu dissipation tests (see Fig. 18). Uniform deposition is also supported by the consistent stratigraphy identified by the boreholes drilled, geophysical and in situ tests. On the other hand, strength anisotropy is frequently evaluated by comparing the undrained shear strength obtained

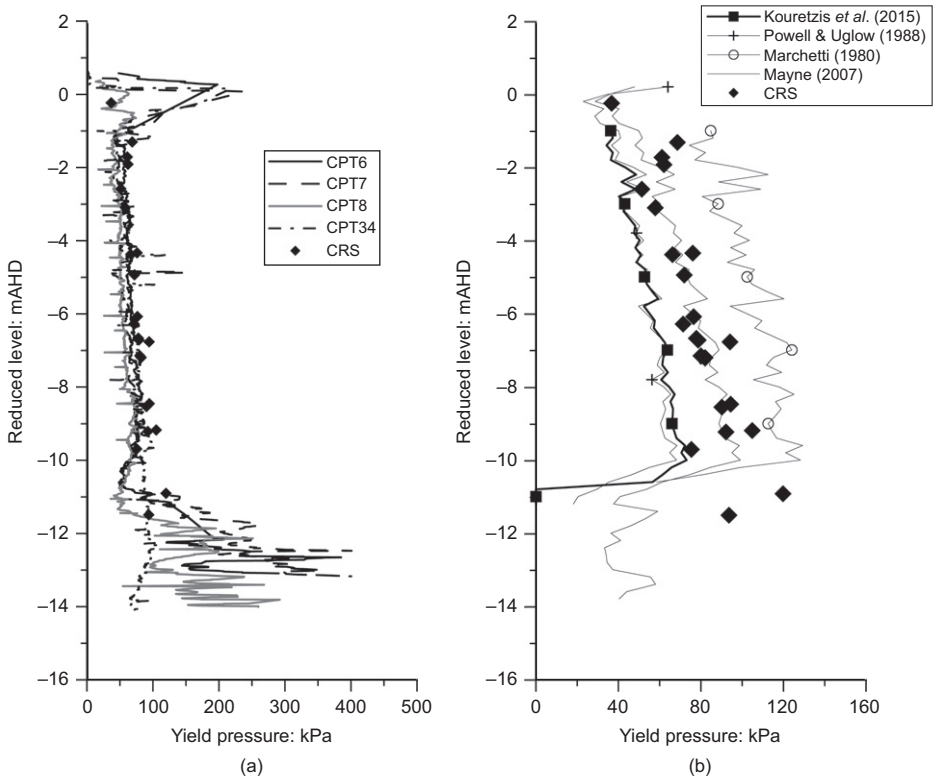

Fig. 14. Estimation of σ'_p. (a) CPTu correlation. (b) SDMT correlation

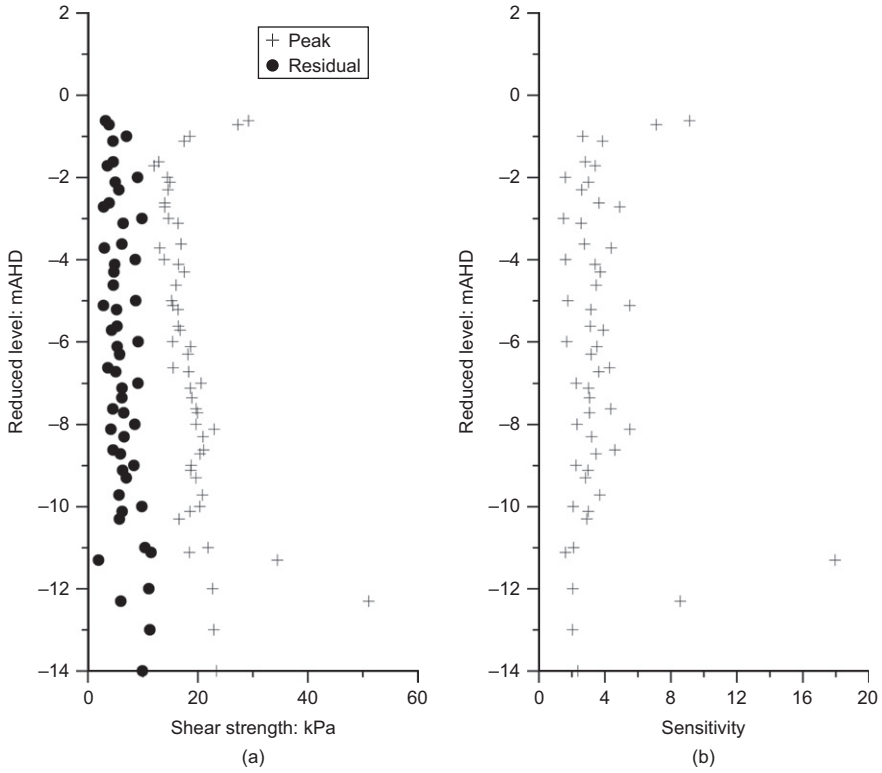

Fig. 15. (a) Shear vane test data. (b) Sensitivity

from compression and extension tests ($s_{u\text{-}TE}/s_{u\text{-}TC}$). Fig. 20 shows values of $s_{u\text{-}TE}/s_{u\text{-}TC}$ based on the results reported by Pineda *et al*. (2016a). The strength ratio is plotted in this figure as a function of the plasticity index. Data obtained from K_0 triaxial compression and extension tests on different natural soft clays compiled by Won (2013), as well as the suggested expressions by Kulhawy & Mayne (1990) for plane strain and triaxial conditions, are included in this figure for comparison. A strength ratio of 0·66 is observed for Ballina clay, which seems to be insensitive to PI. Despite the few experimental data, it suggests that Ballina clay displays some degree of strength anisotropy which lies in the range of

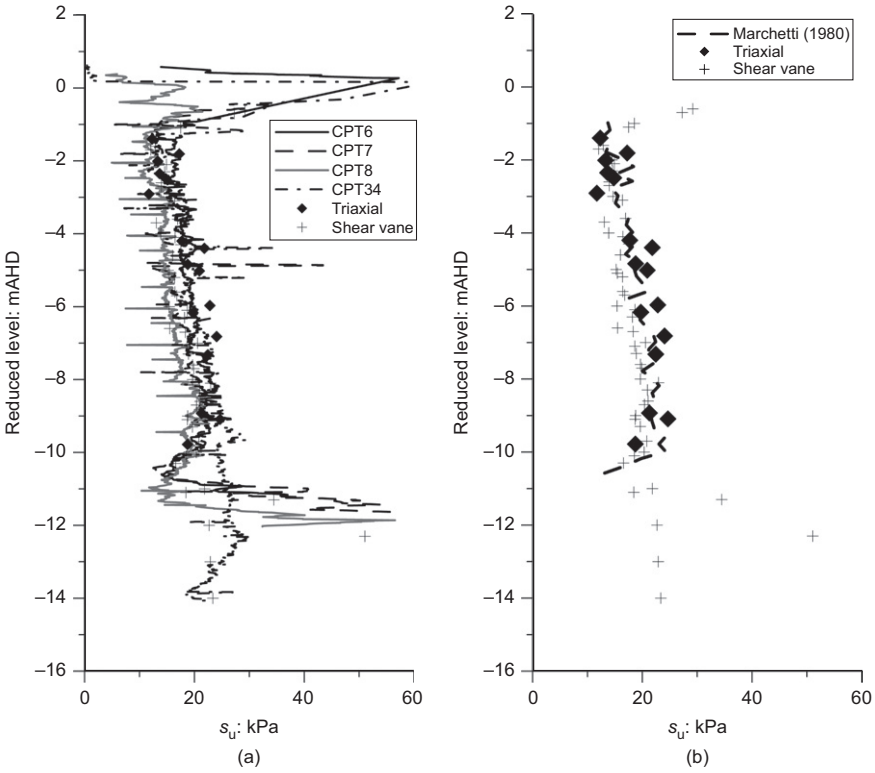

Fig. 16. Estimation of the undrained shear strength from in situ tests. (a) CPTu correlation. (b) SDMT correlation

variation reported in the literature for natural soft clays. However, values reported here for Ballina clay lie below the suggested trend by Kulhawy & Mayne (1990). As observed in Fig. 21, the variation of the undrained shear strength normalised against σ'_{v0} (Fig. 21(a)) as well as in terms of σ'_{yield} (Fig. 21(b)) seems to be consistent with the trends previously reported for soft clays (e.g. Chandler, 1988; Ladd, 1991; Nash *et al.*, 1992).

Undrained shear strength of the Ballina clay, as a function of liquidity index and sensitivity is plotted in Fig. 22. Contours of sensitivity are taken from Leroueil *et al.* (1990) and the range of data is taken from Kulhawy & Mayne (1990). The line for insensitive soils is taken from Atkinson (2007). The data points are from triaxial tests reported by Pineda *et al.* (2016a) and shear vane tests reported in this paper. The Ballina data generally plot within the expected range, although some of the data have a higher strength for a given liquidity index than the range of data. The inferred sensitivity of the Ballina data is approximately 2 to 12 and is higher than shown in Fig. 15(b) (approximately 2 to 6).

The behaviour of Ballina clay appears to be broadly consistent with the behaviour of other clays but undrained shear strength and compressibility of the Ballina clay generally plot at sensitivity contours higher than measured by the shear vane tests. For a given liquidity index, the combination of a high undrained shear strength and high compressibility suggests that Ballina clay could be lightly cemented or connected by organic compounds, although there is no direct evidence in the SEM of this.

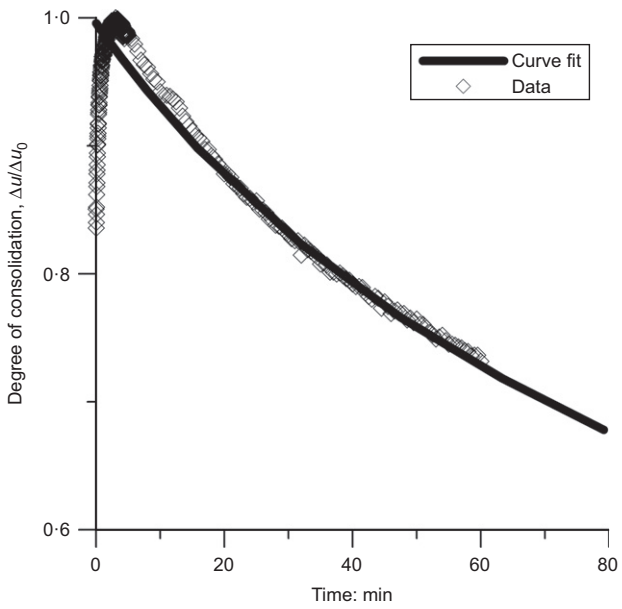

Fig. 17. Typical dissipation curve and fit

CONCLUDING REMARKS

The proposed geological model for the site suggests that the Ballina clay was deposited under saline water in a low-energy estuarine environment over a period of about 8000 years. Relative sea levels have reduced by 1 m to 2 m in the last 3000 years and groundwater levels currently fluctuate by about 1·5 m. The site stratigraphy determined from the geophysical and in situ tests is reasonably uniform, as is the horizontal distribution of the material properties assessed using stochastic methods. Conductivity measurements and sensitivity derived from shear vane measurements indicates that freshwater leaching has not occurred to any significant degree below 3 m depth.

The in situ tests and measurements provided important contributions to identification of the site stratigraphy, groundwater levels and in situ stresses. Published empirical correlations between in situ tests and material parameters

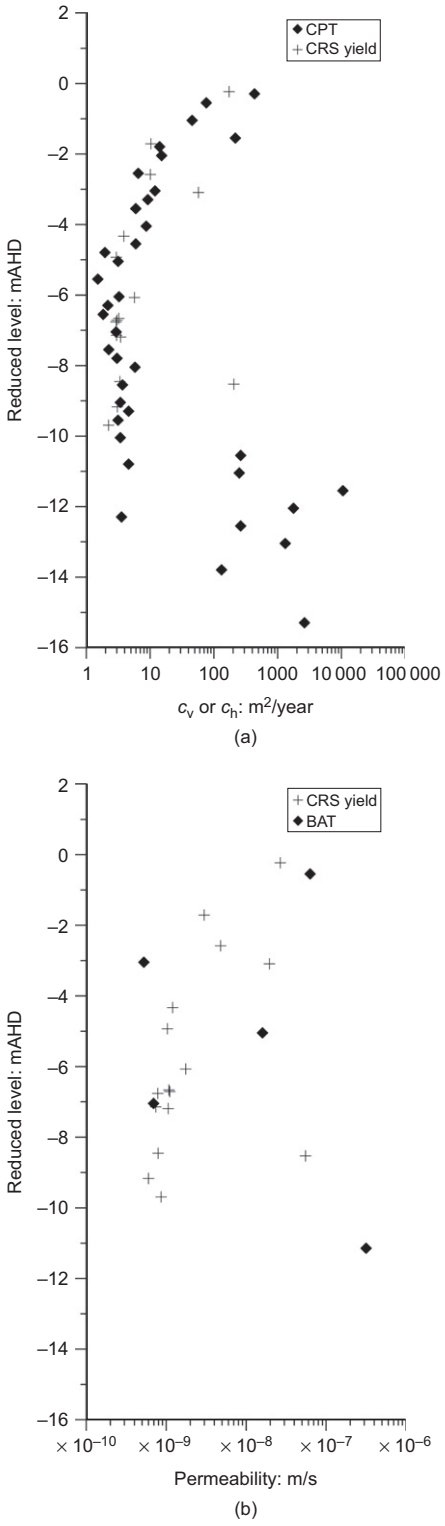

Fig. 18. (a) Consolidation coefficients c_h and c_v. (b) Permeability

indicate relatively good success in predicting the mechanical parameters of Ballina clay obtained from laboratory tests. Use of published SDMT interpretations for K_0 and yield pressure generally resulted in poor correlations with laboratory test data. A close fit between in situ and laboratory test data was obtained where site-specific correlation of the data occurred. The calibration between the CPTu and yield pressure resulted in a factor similar to that reported by Mayne (2007) for a wide variety of soils. N_{KT} values obtained from this study are consistent with published data.

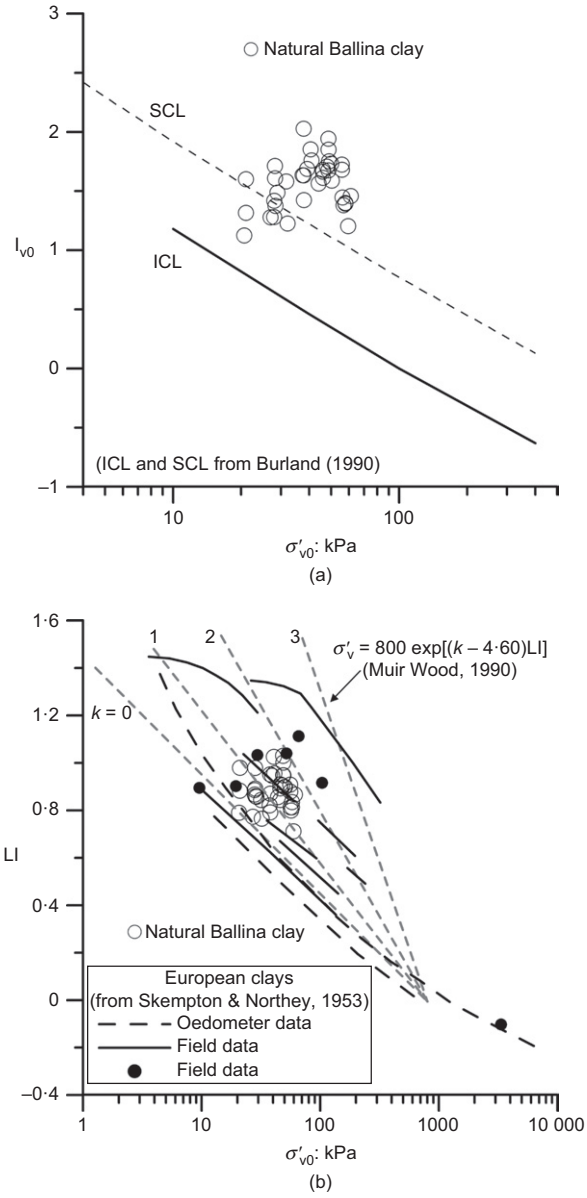

Fig. 19. (a) In situ void index plotted against σ'_{v0}. (b) Liquidity index plotted against σ'_{v0} (modified from Muir Wood, 1990)

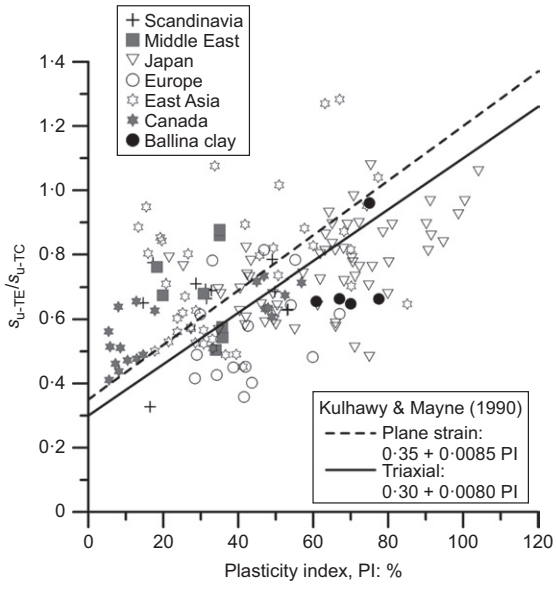

Fig. 20. Strength ratio plotted against PI for natural soft clays

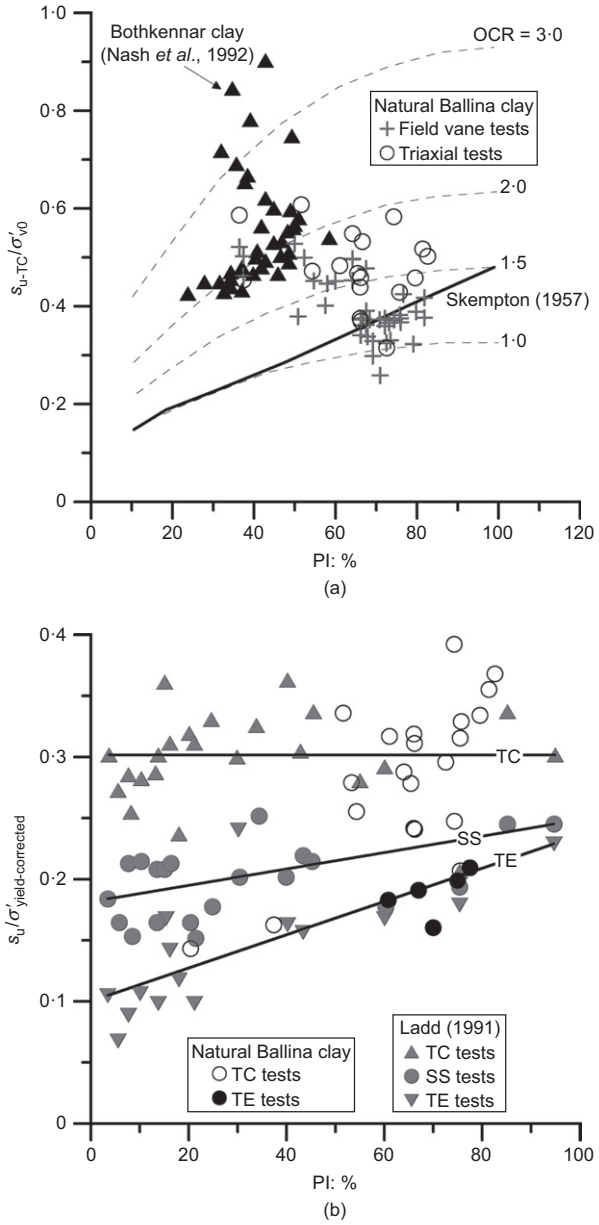

Fig. 21. Normalised shear strength plotted against PI

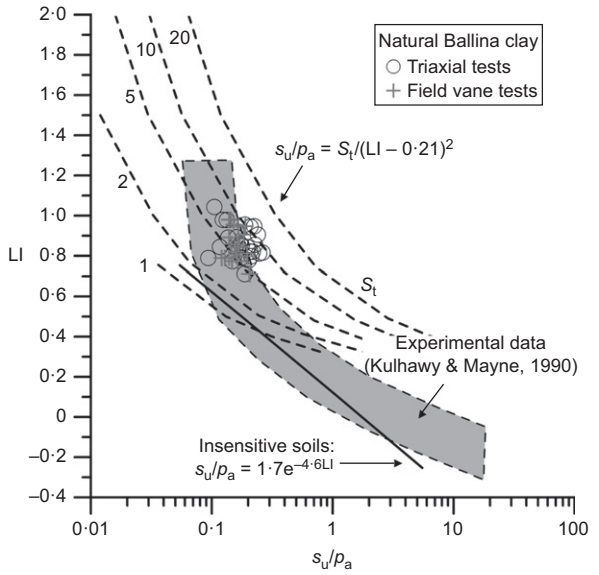

Fig. 22. Undrained shear strength plotted against liquidity index

Given the uncertainties identified with the interpretation of CPTu and SDMT tests, characterisation of material parameters for Ballina clay using these in situ tests and published correlations without reference to laboratory tests should only be considered a first-order estimate.

A combination of in situ and laboratory tests is required for a more accurate site characterisation study. An ideal site characterisation would comprise a programme of high-quality laboratory tests at close depth intervals calibrated to in situ tests at the same location and then a more extensive programme of in situ tests to assess the spatial variability of stratigraphy and material parameters.

It should be noted that the in situ tests are correlated to laboratory tests which have been sampled and tested using certain methods. Pineda *et al.* (2016a) have shown that the yield pressure and undrained shear strength values for the Ballina clay depend on the rate of testing. Interpretation of the in situ test data therefore represents the performance of the ground under laboratory reference strain, strain rate and void ratio conditions, as well as different boundary conditions, strains, strain rates and drainage conditions in situ.

All data presented in this paper will be uploaded to the CGSE (2016) post-publication.

ACKNOWLEDGEMENTS

The Australian Research Council Centre for Excellence in Geotechnical Science and Engineering acknowledges support from Douglas Partners, Coffey Geotechnics, Advanced Geomechanics and the NSW Science Leveraging Fund

NOTATION

B_q	normalised excess pore pressure
C_c^*	coefficient of compression for a reconstituted soil
C_k	permeability change index
c_h	coefficient of horizontal consolidation
c_v	coefficient of vertical consolidation
$c_{v\text{-yield}}$	coefficient of vertical consolidation at the yield pressure
E_D	dilatometer modulus
e_{100}^*	void ratio at 100 kPa pressure for a reconstituted soil
F	shape factor for BAT tests
F_R	normalised friction ratio
F_s	sleeve friction
f	ratio of undrained shear strength to effective vertical stress for normally consolidated clay
G_0	small strain stiffness
G_{50}	secant shear stiffness at 50% of peak shear strain
I_D	material index for SDMT
I_R	rigidity index
I_v	intrinsic void index
I_{v0}	intrinsic void index at in situ void ratio
K_0	coefficient of lateral earth pressure
K_D	horizontal stress index for SDMT
k	empirical constant
k_h	horizontal permeability
k_v	vertical permeability
N_{KT}	correlation coefficient
P_a	normalising pressure taken to be 1 kPa or 100 kPa
$P0$	initial dilatometer pressure reading
P_0	initial system pressure for BAT tests
P_1	inflated dilatometer pressure reading
P_t	pressure at time t for BAT tests
p'	effective mean stress
Q_n or Q	normalised cone tip resistance
Q_{tn}	normalised cone resistance
q_c	cone tip resistance
q_t	net cone tip resistance
Su_{TC}	undrained shear strength in triaxial compression

Su_{TE}	undrained shear strength in triaxial extension
s_u	undrained shear strength
t	time
U_0	static pore pressure
U_2	pore pressure measurement
V_0	initial gas volume for BAT tests
V_s	shear wave velocity
w_{nat}	natural water content
x	power exponent
z	depth
ρ_d	dry density
ρ_{solid}	density of solids
σ'_p	yield pressure (also termed preconsolidation pressure)
σ_v	bulk vertical stress
σ'_v	effective vertical stress
$\sigma'_{v\ yield\ corrected}$	yield pressure corrected for strain rate effects
σ'_{v0}	effective vertical stress at in situ void ratio
ϕ	friction angle

REFERENCES

Atkinson, J. (2007). *The mechanics of soils and foundations*. Abingdon, UK: Taylor and Francis.

BAT GMS (2016). *BAT groundwater monitoring system*. Vallentuna, Sweden: BAT Geosystems AB. See http://www.bat-gms.com (accessed 31/10/2016).

Becker, D. E., Crooks, J. H. A., Been, K. & Jefferies, M. G. (1987). Work as a criterion for determining in situ and yield stresses in clays. *Can. Geotech. J.* **24**, No. 4, 549–564.

Bishop, D. T. (2004). A proposed geological model and geotechnical properties of a NSW estuarine valley: a case study. *Proceedings of the 9th ANZ conference*, Auckland, New Zealand, pp. 261–267.

Bishop, D. T. & Fityus, S. (2006). The sensitivity framework: behaviour of Richmond River estuarine clays. *Proceedings of Australian Geomechanics Society, Sydney chapter mini-symposium*, Sydney, Australia, pp. 167–178.

Bjerrum, L. (1954). Geotechnical properties of Norwegian Marine Clays. *Géotechnique* **4**, No. 2, 49–69, http://dx.doi.org/10.1680/geot.1954.4.2.49.

Burger, H. R. (1992). *Exploration geophysics of the shallow subsurface*. Englewood Cliffs, NJ, USA: Prentice Hall.

Burland, J. B. (1990). On the compressibility and shear strength of natural clays. *Géotechnique* **40**, No. 3, 329–378, http://dx.doi.org/10.1680/geot.1990.40.3.329.

Cao, L., Chang, M. F. & Teh, C. I. (2015). Analysis of dilatometer tests in clay. *Proceedings of DMT'15, 3rd international conference on the flat dilatometer*, Rome, Italy, pp. 385–392.

CGSE (Australian Research Council Centre of Excellence for Geotechnical Science and Engineering) (2016) http://CGSE.edu.au (accessed 31/10/2016).

Chandler, R. J. (1988). The in situ measurement of the undrained shear strength of clays using the field vane. In *Vane shear strength testing in soils: field and laboratory studies (STP1014)* (ed. A. F. Richards), pp. 13–45. Philadelphia, PA, USA: American Society of Testing and Materials.

Colreavy, C., O'Loughin, C. & Randolph, M. (2016). Estimating consolidation parameters from field piezoball tests. *Géotechnique* **66**, No. 4, 333–343, http://dx.doi.org/10.1680/jgeot.15.P.106.

Duncan, J. M. & Buchignani, A. L. (1976). *An engineering manual for settlement studies*. Berkeley, CA, USA: Department of Civil Engineering, University of California.

Foti, S., Lai, C. G., Rix, G. J. & Strobbia, C. (2015). *Surface wave methods for near-surface site characterisation*. Boca Raton, FL, USA: CRC Press.

Gaone, F., Doherty, J. & Gourvenec, S. (2016). Self-boring pressuremeter tests at the national field testing facility, Ballina NSW. *Proceedings of the international conference on site characterisation ISC5*, Gold Coast, Australia.

Hashimoto, T. R., Saintilan, N. & Haberle, S. G. (2006). Mid-Holocene development of mangrove communities featuring Rhizophoraceae and geomorphic change in the Richmond River Estuary, New South Wales, Australia. *Geogrl Res.* **44**, No. 1, 63–76.

Kelly, R. B. (2014). Design and construction of a resilient motorway on difficult ground. *Proceedings of Australian Geomechanics Society, Sydney chapter symposium*, Sydney, Australia, pp. 37–45.

Kouretzis, G. P., Ansari, Y., Pineda, J., Kelly, R. & Sheng, D. (2015). Numerical evaluation of clay disturbance during blade penetration in the flat dilatometer test. *Géotechnique Lett.* **5**, No. 3, 91–95.

Kulhawy, F. H. & Mayne, P. W. (1990). *Manual on estimating soil properties for foundation design*, Report EL-6800. Cornell University: Ithaca, NY, USA.

Lacasse, S. & Lunne, T. (1988). Calibration of dilatometer correlations. *Proceedings of international symposium on penetration testing ISOPT-1, Rotterdam, the Netherlands*, vol. 1, pp. 539–548.

Ladd, C. C. (1991). Terzaghi Lecture – stability evaluation during staged construction. *J. Geotech. Engng* **117**, No. 4, 540–615.

Leroueil, S., Magnan, J. P. & Tavenas, F. (1990). *Embankments on soft clays,* Series in Civil Engineering. Chichester, UK: Ellis Horwood.

Lewis, S. E., Sloss, C. R., Murray-Wallace, C. V., Woodroffe, C. D. & Smithers, S. G. (2013). Post-glacial sea-level changes around the Australian margin: a review. *Quaternary Sci. Rev.* **74**, 115–138.

Li, J., Cassidy, M. J., Huang, J., Zhang, L. & Kelly, R. (2016). Probabilistic identification of soil stratification. *Géotechnique* **66**, No. 1, 16–26, http://dx.doi.org/10.1680/jgeot.14.P.242.

Loughnan, F. C. (1969). *Chemical weathering of the silicate minerals*. New York, NY, USA: Elsevier.

Low, H. E., Landon Maynard, M., Randolph, M. & DeGroot, D. (2011). Geotechnical characterisation and engineering properties of Burswood clay. *Géotechnique* **61**, No. 7, 575–591, http://dx.doi.org/10.1680/geot.9.P.035.

Lunne, T., Robertson, P. K. & Powell, J. J. M. (1997). *Cone penetration testing in geotechnical practice*. New York, NY, USA: Blackie Academic/Routledge Publishing.

Marchetti, S. (1980). In situ tests by flat dilatometer. *J. Geotech. Engng Div. ASCE* **106**, No. GT3, 299–321.

Mayne, P. W. (1995). Profiling yield stresses in clays by in situ tests. *Transpn Res. Rec.* 1479, 43–50.

Mayne, P. W. (2007). *Cone penetration testing state-of-practice*, NCHRP project 20-05. Washington, DC, USA: Transportation Research Board, National Research Council.

Mitchell, J. K. (1976). *Fundamentals of soil behaviour*. New York, NY, USA: Wiley.

Muir Wood, D. (1990). *Soil behaviour and critical state soil mechanics*. Cambridge, UK: Cambridge University Press.

Nash, D. F. T., Powel, J. J. M. & Lloyd, I. M. (1992). Initial investigations of the soft clay test-bed site at Bothkennar. *Géotechnique* **42**, No. 2, 163–181, http://dx.doi.org/10.1680/geot.1992.42.2.163.

Pineda, J. A., Suwal, L., Kelly, R. B., Bates, L. & Sloan, S. W. (2016a). Characterization of the Ballina clay. *Géotechnique* **66**, No. 7, 556–577, http://dx.doi.org/10.1680/jgeot.15.P.181.

Pineda, J. A., Liu, X. F. & Sloan, S. W. (2016b). Effects of tube sampling in soft clay: a microstructural insight. *Géotechnique*, http://dx.doi.org/10.1680/jgeot.15.P.217.

Powell, J. J. M. & Uglow, I. M. (1988). The interpretation of Marchetti dilatometer tests in UK clays. *Proceedings of ICE penetration testing in the UK*, Birmingham, UK, pp. 269–273.

Randolph, M. F. (2004). Characterisation of soft sediments for offshore applications. *Proceedings of international conference on site characterisation, ISC2*, Porto, Portugal, pp. 209–232.

Richards, D. J., Clark, J., Powrie, W. & Heyman, G. (2007). Performance of push-in pressure cells in overconsolidated clay. *Proceedings Instn Civ. Engrs – Geotech. Engng*, **160**, No. 1, 31–41.

Robertson, P. K. (1990). Soil classification using the cone penetration test. *Can. Geotech. J.* **27**, No. 1, 151–158.

Senneset, K., Sandven, R. & Janbu, N. (1989). Evaluation of soil parameters from piezocone tests. *Transpn Res. Rec.* **1235**, 24–37.

Skempton, A. W. & Northey, R. R. (1953). The sensitivity of clays. *Géotechnique* **3**, No. 1, 30–53, http://dx.doi.org/10.1680/geot.1952.3.1.30.

Teh, C. I. & Houlsby, G. T. (1991). An analytical study of the cone penetration test in clay. *Géotechnique* **41**, No. 1, 17–34, http://dx.doi.org/10.1680/geot.1991.41.1.17.

Torstensson, B.-A. (1984). A new system for ground water monitoring. *Ground Water Monit. Remediat.* **4**, No. 4, 134–138.

Won, J. Y. (2013). Anisotropic strength ratio and plasticity index of natural clays. *Proceedings of 8th international conference on soil mechanics and geotechnical engineering*, Paris, France, pp. 445–448.